VIRUS DETECTION USING FILAMENT-COUPLED ANTIBODIES

By

Gregory Philip Stone

Dissertation

Submitted to the Faculty of the

Graduate School of Vanderbilt University

in partial fulfillment of the requirements

for the degree of

DOCTOR OF PHILOSOPHY

in

Biomedical Engineering

December, 2005

Nashville, Tennessee

Approved:

Frederick R. Haselton

Todd D. Giorgio

E. Duco Jansen

Ray Mernaugh

Mark M. McQuain

ACKNOWLEDGEMENTS

I have many people to thank for helping me down the long and sometimes frustrating road through graduate school. Let me start by thanking my advisor, Dr. Rick Haselton, whose funding and support made this project possible. Our weekly meetings not only provided many thoughtful discussions but also helped keep me motivated through many difficult times of the project.

I would like to thank the great friends that I have made during my time at Vanderbilt. They have made my graduate work much more enjoyable, and the social outlet that they provided was critical to my happiness in graduate school. I would especially like to thank the numerous roommates that I have had in Nashville who have always made my house an enjoyable place to be, including Rob, Steve, Adam, Jonny, Dave R., and Dave C. I have met so many others in Nashville whose friendship I greatly appreciate, and without these valuable relationships, I never could have made it all the way to my PhD.

My fellow lab mates in the Haselton and Giorgio labs have not only been a source of friendship, but also of frequent scientific advice and ideas. Ash was a major motivating factor for me and made all the late nights in the lab much easier. Although the source of frequent aggravation, he was always a reliable dinner companion and partner for burning the midnight oil. In the Giorgio Lab, Sam was a constant target of my inquiries for both scientific and non-scientific topics and was always full of useful information on whatever happened to be my question of that day. All the other

Haselton and Giorgio lab members made the lab an enjoyable place to work, and I thank them for that.

I would also like to thank Jarntip for her constant support over the last three years. She has given endless encouragement during the tough times and has always tried to help me stay positive when I was struggling. The thousand miles that have been between us for the last two and a half years did not lessen the amount positive reinforcement during frustrating times, and helped motivate me to finish my degree as soon as possible.

Finally, I need to thank my parents for their love and support over the last 29 years. Their unwavering love and support over the years allowed me to follow my own career path without ever letting me feel that something was out of reach or not good enough. They provided me with every advantage in life to help me achieve my goals, and I credit them for helping shape me into the person that I am today. For their steadfast love and support, I say “thank you”.

TABLE OF CONTENTS

Appendices

LIST OF FIGURES

LIST OF TABLES

CHAPTER I

INTRODUCTION

This work has been divided into six major chapters. Chapter 1 provides a brief description of the organization of this dissertation along with a summary of the three major specific aims of this project. Background information for virus detection strategies along with the significance of this project are described in Chapter II. The bulk of this dissertation is comprised of three manuscript chapters, each corresponding to one of the specific aims. Chapter III is my first report covering the basic aspects of my filament-based virus detection system. This manuscript was published in the September 20, 2005 issue of *Biotechnology and Bioengineering*. The second report on my virus detection system comprises Chapter IV. This manuscript focuses on the successful development and implementation of an integrated fluorescence detector into my virus detection system, along with the incorporation of an adaptive feedback mechanism. This manuscript was submitted for review to the *Journal of Biomedical Optics* in December, 2005. My final manuscript comprises Chapter V. The focus of this final manuscript is the incorporation of a small set of human pathogens (reovirus) to show progressive detection of virus along a pre-programmed theoretical decision tree. The manuscript describes a true feedback mechanism where current results are fed back to the control program to guide further testing to achieve specific diagnosis of virus subtype. This manuscript will be submitted to the *Journal of Immunological Methods* in December

2005. The final major chapter includes a brief write up of the potential applications for this technology, along with some future directions (Chapter VI).

Specific Aims

The major goal of this work was to develop a filament based virus detection platform that uses passively immobilized antibodies on the surface of a monofilament. The antibody regions are pulled through a series of reaction chambers where virus is detected with a fluorescently labeled second antibody, and the filament is scanned for fluorescence using an integrated detector. This work was divided into three major design and development stages that are summarized below.

Specific Aim 1: Design an automated virus detection platform using offline fluorescence detection and a single antigen/antibody pair

The goal of this aim was to use a single virus/antibody pair to show that antibody probes could be immobilized on the surface of a monofilament and maintain their ability to capture target molecules out of solution. This aim was separated into several major design issues: filament selection, probe immobilization, chamber design, reaction conditions, and filament control. Selection of the optimal filament was critical for adequate probe attachment. Several potential filaments were identified and were evaluated based on composition, size, autofluorescence, and solvent compatibility. A polyester monofilament was a good choice for preliminary work. Consistent deposition and attachment of probe to the chosen filament was an essential factor for achieving consistent and quantifiable results with my system. Next, chamber design determined reaction volumes, diffusion distance, and fluid loss between adjacent reaction chambers.

Finally, automated filament control was necessary to minimize user intervention and allow easy programming of basic filament movement patterns.

Specific Aim 2: Develop an integrated fluorescence detector and feedback controls

The main goal of this aim was to develop an integrated fluorescence detector so that filaments could be immediately scanned following virus detection experiments. Online fluorescence detection allowed fluorescence data to be passed back to the control program for analysis, which enabled adaptive feedback control. In this system, filament regions of interest were sent back through the reaction chambers for additional incubation if signal strength was inadequate. We defined several hardware and software requirements to complete this aim of the project. The choice of a suitable excitation light source, detector, filter sets, and digital acquisition board was the first step. Software requirements included the ability to coordinate filament control with digital data acquisition, so that adaptive feedback was possible.

Specific Aim 3: Characterize an unknown virus sample by incorporating a priori *knowledge of antibody specificity to reovirus*

A pathogen with established subtypes that exhibit differences in protein expression and reactivity was needed to test the feedback and decision capabilities of this technology. Reovirus provided a well-characterized pathogen with several known strains and serotypes. Using *a priori* knowledge of differences in antibody affinity towards reovirus subtypes, a simple decision tree was designed that tested samples with different specificity, depending upon the results at each branch of the tree. As a general strategy,

the specificity of testing progressed from low (top level of testing) to high (bottom level of testing). The decision tree guided testing, so that in appropriate situations, unnecessary testing of every branch in the tree was avoided. We identified a set of reoviruses and corresponding antibodies that were suitable to use in the decision tree.

CHAPTER II

BACKGROUND

Rationale

Recent media attention concerning the possibility of a world wide flu pandemic has brought to light many issues involving the preparedness of both local and national authorities to initiate an effective response to a viral outbreak. In addition, many experts believe that a major threat to our country lies in the area of biological warfare due to the ease with which numerous deadly bacterial and viral agents can be obtained or produced (1-4). The first step in mounting an effective response is fast and reliable detection of a wide variety of pathological agents. Numerous laboratory techniques exist that, when used in conjunction with each other, can detect nearly any known human pathogen. However, none of these techniques is effective for all pathogens, and each has its own shortcomings. A universal virus detection platform that can detect a wide range of pathogens with a high degree of sensitivity and accuracy is highly desirable

Current Detection Methods

Virus Culture and Microscopy

Traditional culturing of virus in cells has been used for a long time for the growth and isolation of virus, but it still remains an important method of virus detection. In fact there are many clinically important viruses that can be grown in just a small set of cell

lines. This method typically involves infecting the cells and monitoring the characteristic cytopathic effect through light microscopy, but not all relevant viruses are easily cultured, such as hepatitis virus, Epstein-Barr virus, and HIV. In addition, some viral antigens may remain with the host much longer than live, intact virus, so testing may need to be performed early in an infection before viral shedding becomes too low (5). The significant time lag between infection of cells and diagnosis, along with limited sensitivity, are major reasons why this technique is losing ground to more sensitive molecular based techniques (1,6).

Electron microscopy has the major advantage that it is theoretically able to detect all viruses directly in a sample or by the cytopathic effect on cells in a sample, making virus culture unnecessary. But EM has very low sensitivity, requires a very expensive capital expenditure, and requires skilled personnel to make an accurate diagnosis.

Serology

Serology is based on the fact that a humoral response will always follow an infection. It is based on a rise in antibody titer from the beginning of an infection to the end, and serum collection typically is separated by at least 10-15 days. ELISA is commonly used for serological testing, but typically the virus itself is immobilized in a microtiter well instead of an antibody. Immobilized virus binds antibody from the sample and a labeled secondary antibody is used for detection. Serology is typically used when other methods of virus detection are not feasible or effective or when viral shedding has reduced so much that other techniques are not effective. Antibody response varies, but antibodies will be present in high amounts long after viral shedding has nearly

ceased. The major drawbacks are the time delay between serum collections and the low sensitivity due to cross reactivity of many antibodies and antigens (5).

Antigen Detection

Immunofluorescence (IF). IF typically utilizes a fluorescently or enzyme labeled anti-viral antibody to bind to the virus in a sample. Detection can be done through absorption or fluorescence readings using a microtiter plate or fluorescence microscope. These assays are typically quick (1-2 hrs) and are more sensitive than viral culture techniques. However, a quality sample is needed due to cross reactivity of many antigens and antibodies. IF is often used to diagnose respiratory viral infections such as respiratory syncytial virus (RSV), parainfluenza, and influenza using a nasopharyngeal aspirate. Since viral antigens are displayed on the surface of epithelial cells for these viruses, at least a minimum number of cells is required for adequate detection. This requires trained personnel to obtain and prepare a quality sample and, for some viruses, limits the sensitivity of this technique (5).

Solid Phase Assays

ELISA. The enzyme linked immunosorbent assay (ELISA) is a widely used technique because of its simplicity and lack of expensive processing and detection equipment. In a typical ELISA, a capture antibody is immobilized by passive adsorption into wells of a polymer microtiter plate and binds antigen in solution. Next, a detecting molecule is added to each well that is coupled to a color-producing enzyme such as horseradish-peroxidase (HRP), followed by the addition of a chemiluminescent reagent.

ELISA is a very useful technique, but reagents are typically pipetted by hand into each well and a typical assay may utilize all 96 wells of a 96-well plate. In addition, sensitivity remains poor compared to IF. ELISA can be very time consuming and labor intensive, taking up to 12 hrs to achieve adequate signal. As a result, experimental throughput is very low.

Antibody Arrays. Antibody arrays are able to probe in parallel for many viral antigens. The theory of these arrays is similar to DNA arrays in that an array of antibodies is immobilized on the surface of a substrate, and a labeled target solution is washed across the surface to identify select components through antibody/antigen interactions.

Antibody arrays suffer from several shortcomings that have prevented their widespread use thus far. Many commercially available antibodies are not suitable for use as probes due to lack of specificity and sensitivity. Many antibodies will cross-react with numerous other cellular proteins, so signal intensity is not always directly linked to a specific protein abundance. Finally, protein labeling can often interfere with its binding epitope, another factor that will limit antibody/antigen interactions (7). Antibody selectivity must be greatly improved before antibody arrays can become a more integral tool for viral antigen detection (7).

Nucleic Acid-Based Techniques

PCR. The polymerase chain reaction (PCR) has found widespread use in clinical and research settings because it can detect very low abundance molecules. It has been reported that molecules with a copy number of only 1 molecule/ml have been detected,

but a typical PCR requires anywhere from 10-100 molecules (8). The molecule of interest is amplified through repeated heating and cooling cycles in the presence of certain enzymes and excess nucleotide bases. As a result, the sensitivity of PCR is unmatched by any other technique, but contamination by foreign DNA that is recognized by the same primers can create large background signals. Analysis of final product is often done using a DNA gel or by hybridizing to a labeled complementary DNA strand.

Since all viruses contain DNA or RNA, PCR could, in theory, be used for any virus, but well designed primers are needed for effective amplification. A good understanding of primer requirements is necessary since one primer may good for one variant of a virus but not another. Primer designing software is available to aid in the development of good primers since secondary structure in a primer can prevent proper hybridization. Real time PCR has been developed that monitors fluorescence produced as the amplification reactions proceed, which makes gel analysis unnecessary. This process can be very fast and sensitive (5,6,9).

Another attractive feature of PCR is that active viruses are not needed, so sample transport and storage is less of a problem with this technique. However, RNAses that are present can often damage sample. Sample preparation is extremely important for PCR due to the extreme sensitivity of the technology. Contamination from previous samples or environmental contamination is always a major concern. As a result, dedicated PCR preparation areas and tools are required that are isolated from other laboratory functions are necessary to prevent contamination.

DNA Arrays. DNA microarrays are based on the sequence complementarity of the two DNA strands (10-14). When separated, complementary DNA strands reassemble

with extraordinary accuracy. The concept of using labeled nucleic acids in solution to interact with known probes attached to a solid support has been around for many years. With the incorporation of solid, non-porous supports such as glass, the process was easily miniaturized in the form of DNA microarrays (15,16). DNA microarrays can be synthesized containing arrays of spots numbering from 10,000 to over 100,000 in one array (17-19). DNA arrays could be an excellent way to probe for thousands of specific viral genes or gene segments, but sensitivity is not high enough to directly detect viral DNA. Since sample preparation is required before hybridization can be performed, DNA microarrays are not as useful for directly probing biological fluids for viral nucleic acids.

Limitations of current strategies

Single molecule strategies. Techniques such as virus culture, IF, PCR, and ELISA can be quite useful for identifying the presence of a small set of viruses or viral antigens within a sample. These methods often require relatively inexpensive equipment and can be very effective when the required sample throughput is low. However, when probing for an increasing number of viruses and viral antigens is required, these techniques become much less cost effective in terms of reagents and labor costs.

Global detection strategies. The purpose of global techniques is to probe for as many viral antigens or nucleic acid segments as possible in a single assay, but this approach does not come without a cost. The requirement of higher sample volumes can be a critically limiting factor when using these techniques in a clinical setting where patient samples are limited. Dynamic range is also a major problem of this all-in-one approach. Since all spots are processed simultaneously under the same conditions, there

is no accommodation for low or high abundance targets. Longer processing to detect low abundance molecules causes saturation of signal for high abundance molecules, which can mask surrounding spots; however, adjusting the processing for high abundance molecules limits detectability of low abundance molecules. This limitation can sometimes limit the selection of molecules being screened with each technique.

There is an inherent design flaw for array technology that sacrifices quick assay times for better sensitivity. Current DNA and protein arrays are based on an approach where the probes are fixed in space and then exposed to target. Since binding of probe to target requires direct contact, this approach is greatly limited by the slow diffusion of the target molecules across the surface of the array. It has been shown that the diffusion coefficients for DNA and proteins in aqueous solution range from 10^{-6} to 10^{-7} cm^2/s (20-22). For low abundance targets, it is imperative that each probe encounters each possible complementary target to achieve detectability. However, the surface area of most arrays is far too great relative to the low diffusion coefficients for this to occur in a reasonable time frame. In fact, in a typical overnight 12-hour incubation, diffusion of only a few millimeters occurs, so each probe will only interact with a small fraction of available targets. This is a major factor that limits the sensitivity of these assays. As a result, most assays require 20-50 μg of unpurified sample, which is often not feasible (23,24). The typical sensitivity of DNA microarrays ranges from several hundred to a few thousand copies, depending on the assay, and protein arrays typically suffer from even worse sensitivity. They often require many thousands of copies to achieve a detectable signal (BD Clontech, Ray Biotech technical data).

A high-density microarray with the capacity to contain 100,000 spots is overkill when a subset of only 50 structures has been identified as relevant for a particular situation. Probing for irrelevant targets complicates data analysis and wastes time, money, and reagents. Better techniques are needed to effectively and efficiently probe for known pathogen subsets that are too large for most single molecule detection schemes and too small for global detection strategies.

Filament Based Virus Detection System

This work describes a technology that takes an intermediate approach that directly probes for known viral subsets containing tens to hundreds of possibilities. The system directly probes for known viral antigens using immobilized probes on a monofilament. Figure 3 (p.30), Figure 9 (p.55), and Figure 16 (p.90) show simple diagrams of our system. A monofilament with antibody probes on the surface is pulled sequentially through a series of reaction chambers, one of which contains the unknown sample. After a short incubation in that chamber, the probes on the filament are moved through subsequent chambers, washed, incubated with a detecting molecule, and washed again. After processing is complete, the probes of interest are moved through the detector where fluorescence of bound detecting molecule is measured. The movement of the immobilized probes through each reaction chamber is controlled by a motor and computer interface. The number of viral antigens that can be probed is limited only by the number of immobilized antibody spots on the filament.

Advantages of Filament Based System

Reduced volume and diffusion distance

One of the most important consequences of the filament-based design is that diffusion distance required for target molecules to encounter probes is greatly reduced. Since the filament is pulled through the chamber, each probe encounters the entire axial length of the target solution. The result of this filament movement is that target molecules need only to diffuse radially between the filament and the wall of the capillary. Using a small-bore glass capillary with an inner diameter of 300 μm with a 120 μm monofilament reduces the diffusion distance to 90 μm. This distance is orders of magnitude smaller than the centimeter scale required for many techniques such as DNA and protein microarrays. The calculated diffusion time at this scale could occur in minutes as opposed to the many hours required for larger scale systems.

Another consequence of the capillary reaction chamber is the ability to use very small sample volumes. The volume of the capillary lumen is inherently very small, but filament running through the lumen reduces the volume even further. For the dimensions described above, only one or two microliters of target solution is required to fill the chamber. Typical DNA and protein arrays often require 50 μl or more for effective hybridizations. The use of even smaller bore capillary tubes will reduce the diffusion distance and volume requirement even further.

Automation and Feedback

The linear design of this system allows the incorporation of a unique automation and online feedback system that is impossible with other techniques. The system of micro-reaction chambers is attached to the top of a stage, and the filament is attached to a rotating axis. The rotating axis is controlled through a LabView Virtual Instrument that winds and unwinds the filament to move the probe spots through each chamber and through the detector as desired (Figure 9). The first chamber is a blocking chamber containing a low concentration of detergent that serves to prevent the bare filament from non-specifically binding virus or other proteins. As the probes pass through chamber 2, they capture virus out of solution, followed by a quick wash in chamber 3 to get rid of any unbound virus. Chamber 4 contains the detecting molecule that will bind to the captured virus, and chamber 5 provides a final wash to eliminate all unbound molecules from the filament. Finally, the probe is moved through the detector where fluorescence of the detecting molecule is measured.

Since each probe can be processed and controlled independently, reaction conditions can be optimized for each different probe/target pair. Processing of probes for targets expected to be in high or low abundance can be adjusted to keep signals detectable while keeping them all on the same scale. This ability extends the dynamic range of the system so that it is much wider than other technique. In addition, individual spot processing allows for a feedback system in which signal intensity must reach a pre-defined level before continuing to the next probe. If measured signal is too low, that probe spot can be sent back through the reaction chambers for additional processing to improve signal to noise ratio.

Online feedback gives the system its most unique capability. It allows our system to follow a pre-designed decision tree based on prior knowledge of virus and subtypes. In this design, the result from one antibody region determines which region will be processed next. This eliminates unnecessary processing of probes that are shown to be irrelevant based on previous probes. A simple example of this would be in the diagnosis of a particular subtype of an infectious agent. The first set of probes determines the presence of absence of a general pathogen. Following a positive result, probes that differentiate between pathogen subtypes are processed. Using this strategy, each level of the decision tree further characterizes the virus in the sample. This approach eliminates much of the unnecessary probing for irrelevant molecules.

Initial Design Issues

Probe Immobilization

Many of the aspects of this technology are largely unexplored. However, attachment of antibody probes to polymer substrates is one important aspect for which there is a considerable body of literature. Many of these molecular recognition techniques such as DNA arrays, protein arrays, and ELISA require the immobilization of probes to the surface of substrates such as glass or various polymers. Polyester filaments are similar to the polymers used in ELISA, so techniques used to immobilize proteins onto polymer substrates are of great interest. Several methods have been characterized in the literature (25-27), and three have been shown to successfully immobilize antibodies on a polystyrene substrate. These include passive physical adsorption through hydrophobic interactions, chemical immobilization on a polylysine coating, and non-

covalent linkage using a linker protein (protein G) that was passively adsorbed on the surface. Each of these methods was shown to effectively immobilize antibody on the surface while retaining at least some of the antibody's antigen capture ability.

Previous reports showed that antibody density on the polystyrene surface reached a maximum value as the concentration of antibody in the incubation solution increased past certain levels. However, the maximum density of antibody using chemical linking to a polylysine coating was significantly higher than using the other two methods (25,26). In studies of reactivity of immobilized antibody, there exist conflicting reports. There is agreement that an optimal arrangement for antibodies on the surface is the "ends on" configuration where the Fc portion is bound to the support while the Fab portion is left free to bind antigen. Schramm *et al*. have shown that for a particular antibody density, antigen binding is considerably lower for passively adsorbed antibody. However, at increasing densities this discrepancy becomes smaller. They hypothesize that at low antibody density, antibody binds in all configurations including "ends on". As density increases, attachment begins to favor the "ends on" attachment to maximize the amount of antibody that can bind. This helps to free the binding paratopes of the antibodies until the density reaches a point where steric hindrance between binding sites and between binding sites and antigens causes signal to decrease (Figure 1). Non-passively adsorbed antibodies are already bound by their F_c region, so the proportion of available antigen binding sites does not change appreciably at higher densities. Even at the highest density, non-passively adsorbed antibodies exhibit greater binding capacity possibly because of the flexibility imparted by such linking molecules. The work of Butler *et al*. shows an even greater difference between passive and non-passive antibody adsorption. Their

work estimates that as little as 3% of antibody binding site are available to bind antigen after physical adsorption, while up to 70% are available after immobilization using a chemical linker. There is clear agreement that using a linker to immobilize protein results in greater activity of the enzyme or antibody, but the extent to which this is true is not clear.

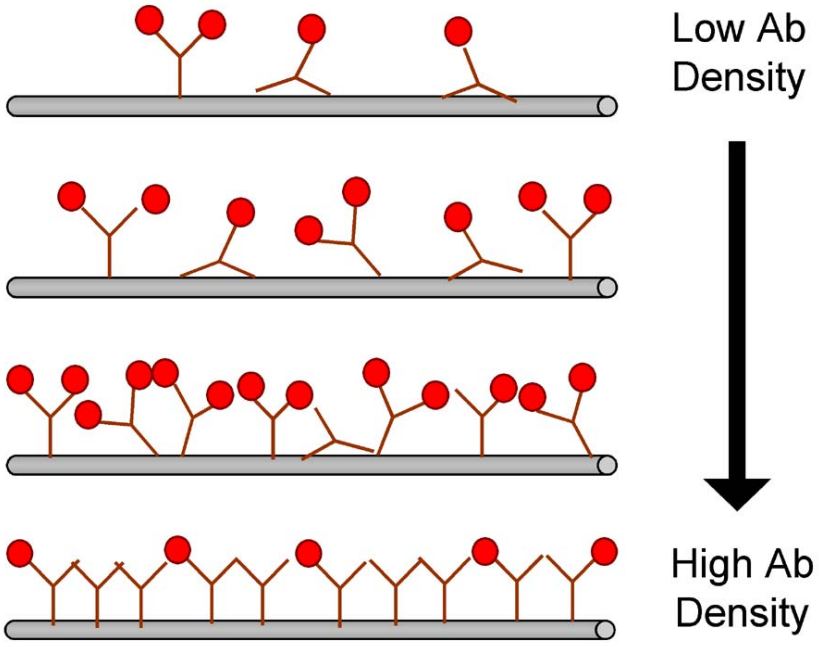

Figure 1: Bound antigen increases with the immobilized antibody density until the density reaches a point where steric hindrance limits antigen interaction.

Virus Test System

M13K07 bacteriophage. A major requirement for the development of this system was selecting a suitable virus test system that can show the full capabilities of our detection platform without any major safety concerns. We chose a single antigen/antibody pair to show the initial automated virus detection during early development. For this, we chose M13K07 bacteriophage due to availability and safety of this virus. Anti-M13K07 monoclonal antibody is available commercially and has a very high affinity for the M13K07. Since anti-M13K07 is a mouse IgG, it should display similar characteristics to other IgGs that will be used later for more complex testing.

In order to show clinical relevance of our system, later testing of our system required more than one virus/antibody pair so that the unique feedback capability could be demonstrated using a set of human pathogens. Through collaborations with Terry Dermody in the Department of Pediatric Infectious Disease, we chose a small subset of reoviruses for testing.

Reovirus. We chose reovirus as a test system due to the expertise on this virus that was available to us, along with the availability of numerous reovirus types and subtypes. Antibodies showing differing levels of specificity toward each type and subtype were either available, or we were able to produce them using existing hybridoma lines. The use of reovirus provided a human pathogen to show the detection and feedback capabilities of our system, while alleviating many of the safety concerns of most human pathogens.

Reovirus is a non-enveloped virus containing 10 double stranded RNA segments. Although reovirus is able to infect mammals, it is rarely associated with adult disease.

Nevertheless, reovirus infection of newborn mice is one of the most commonly used viral models to study mechanisms of infection, pathogenesis, virulence, and viral tropism. Reovirus is both a respiratory and enteric virus, and these are the two known avenues for infection. These routes of infection can lead to numerous diseases such as encephalitis, hydrocephalus, hepatitis, pneumonitis, and myocardis (28-31). Viral spread throughout the host is one of two major pathways: spread through the nerves, or spread through lymphatics and the bloodstream to distant target organs. Each of the predominant reovirus types favors one of these routes, but the mechanisms by which they differ are not completely understood.

The first viruses were isolated form the gastrointestinal tract of animals and humans, although they were not associated with disease in humans. As a result, these viruses were given the name REO, which stands for respiratory enteric orphan virus. Three serotypes have been identified based on their effect on hemagglutination of blood, and the separation of reovirus into these serotypes has been useful in predicting differences in pathogenesis. In addition, each serotype is further characterized by the individual strain, and the four most common prototype strains, representing the three distinct serotypes, have all been isolated from humans: T1 Lang (T1L), T2 Jones (T2J), T3 Abney (T3A), and T3 Dearing (T3D).

Reovirus Protein Coat. Virions contain 11 different proteins that are encoded by 10 discreet dsRNA segments of three distinct size classes. Of these eleven proteins, three are not associated with the virus structure and are not well understood. However, the remaining eight proteins have all been isolated, and their roles in reovirus infection have been studied extensively. These eight structural proteins form two concentric,

intercalating shells, where each protein plays a specific role in reovirus infection. The concentric shells are further defined by function. The outer capsid gives the virion stability and is responsible for interaction with host cells, while the inner core plays a role in cell penetration, release of the viral genome into the host cell, and RNA transcription.

Four major proteins comprise the outer capsid; however, a majority of the capsid is made of the σ3 and μ1 proteins, whose abundance on the outer surface is approximately 600 copies each. The μ1 protein is thought to mediate virus attachment to host cells, while σ3 is thought to play an important role in the release of the virus subparticle once inside the cell. Present at each of the twelve vertices of the icosahedral virion are pentamers of λ2, which are important during RNA synthesis. The final major protein of the outer shell is the σ1 protein, a critical protein for the reovirus virion. It has been closely linked to viral attachment to cells, along with other reovirus properties such as tropism within the nervous system, and different spreading pathways within the body. The remaining structural proteins make up the viral core and play different roles in virus infection and pathogenesis within the body. There are still many interactions among the different reovirus proteins, as well as between viral proteins and the host cell that are not completely understood.

Reovirus Selection and Antibody Specificity. As a human pathogen, the use of reovirus gives clinical relevance to this virus detection platform. Test viruses include T3D, T1L, T3SA+, and T3SA- because they represented two distinct serotypes along with two additional subtypes of serotype three. As a well-characterized virus, antibodies have been created that display both serotype specific and non-serotype specific behavior. Reovirus antibodies that will be used for specific aim three are 9BG5, 5C6, 4F2, and

8H6. While 9BG5 is specific for all serotype three reoviruses, 4F2 shows increased specificity for only T3D reovirus in our scheme. 5C6 is serotype one specific, and 8H6 shows no serotype specificity. This set of reoviruses and antibodies, along with the M13K07 and anti-M13K07, allowed us to design a three level decision tree to demonstrate feedback capabilities of our virus detection platform.

CHAPTER III

VIRUS DETECTION USING FILAMENT-COUPLED ANTIBODIES

Gregory P. Stone[1]
Ray Mernaugh[2]
Frederick R. Haselton[1]

[1]Biomedical Engineering
[2]Department of Biochemistry
Vanderbilt University
Nashville, Tennessee

(This work was published in the September 20, 2005 issue of *Biotechnology and Bioengineering*)

Abstract

Two attractive features of ELISA are the specificity of antibody-antigen recognition and the sensitivity achieved by enzymatic amplification. This report describes the development of a non-enzymatic molecular recognition platform adaptable to point-of-care clinical settings and field detection of biohazardous materials. This filament-antibody recognition assay (FARA) is based on circumferential bands of antibody probes coupled to a 120 μm diameter polyester filament. One advantage of this design is that automated processing is achieved by sequential positioning of filament-coupled probes through a series of 25-60 μl liquid filled microcapillary chambers. This approach was evaluated by testing for the presence M13KO7 bacterial virus using anti-M13KO7 IgG_1 monoclonal antibody coupled to a filament. Filament motion first positioned the antibodies within a microcapillary tube containing a solution of M13KO7 virus before moving the probes through subsequent chambers, where the filament-coupled probes were washed, exposed to a fluorescently labeled anti-M13K07 antibody, and washed again. Filament fluorescence was then measured using a flatbed microarray scanner. The presence of virus in solution produced a characteristic increase in filament fluorescence only in regions containing coupled antibody probes. Even without the enzymatic amplification of a typical ELISA, the presence of 8.3×10^8 virus particles produced a 30-fold increase in fluorescence over an immobilized negative control antibody. In an ELISA comparison study, the filament-based approach had a similar lower limit of sensitivity of $\sim 1.7 \times 10^7$ virus particles. This platform may prove attractive for point-of-care settings, the detection of biohazardous materials, or other applications where sensitive, rapid, and automated molecular recognition is desired.

Introduction

The enzyme linked immunosorbent assay (ELISA) is one of the most common antibody based molecular recognition assays in the laboratory, but the requirements of many clinical applications, where speed and throughput are critical parameters, have exceeded the capability of traditional plate-based ELISA. Automated systems have overcome these limitations in large hospital settings and can process hundreds of samples per hour (32,33). However, large integrated systems are not practical for point-of-care clinical settings where cost is a prohibitive factor. In these settings, samples often are sent off-site for analysis, adding a significant time lag before results are in hand. In many situations, the need for quick diagnosis and treatment make onsite testing very desirable. Many viruses are more easily treated when diagnosed early, so quick and reliable diagnosis that can be performed while a patient waits could allow treatment to begin immediately and, thus, improve the efficacy of treatment. In addition to clinical testing, many field applications exist where rapid identification of a hazardous material is required to formulate an appropriate response.

The generation of monoclonal antibodies and the advent of recombinant DNA technology have significantly increased both speed and sensitivity of molecular based assays (34,35). A number of schemes based on the sandwich immunoassay have been reported in the literature. For example, several recent applications are based upon changes in electrical properties as antigen binds to an immobilized probe (36-39) or based on the interaction of evanescent light waves with surface-bound antibodies (39-42). Many of these approaches are either labor intensive or require complex microfluidic devices and are not well suited for point-of-care clinical diagnostics or for field testing

for biohazardous materials. A simpler antibody-based detection assay would be very desirable.

This report uses a model bacteriophage/monoclonal antibody system to demonstrate a simple sandwich immunoassay that is based on immobilized antibody probes along a polyester monofilament. M13K07 virus and anti-M13K07 IgG provide a simple test system for initial studies. M13K07 is a harmless phage, so experiments can be performed with minimal safety concerns. In addition, highly specific antibodies to M13K07 are commercially available, and binding between virus and antibody is well-characterized. The advantages of this approach include a reduction in reagent volumes and incubation times compared to standard ELISA, along with automation of the reaction process and elimination of the enzymatic amplification required in ELISA. This paper describes the initial studies using this design and compares its sensitivity to traditional plate-based ELISA.

Methods

Reagents

Anti-M13 monoclonal IgG_1 (anti-M13) and anti-E tag monoclonal IgG_1 (anti-E) were obtained from Amersham Biosciences (Piscataway, NJ) and fluorescently labeled with Alexa Fluor 647 (AF647), Alexa Fluor 555 (AF555) (Molecular Probes, Eugene, OR), Cy3, or Cy5 (Amersham Biosciences). Labeling procedures were performed according to the manufacturers' instructions. The concentration of the labeled antibody along with the degree of labeling was calculated from the absorbance at 280 nm and the

peak label absorbance. A working solution of labeled antibody was stored at 4°C, and aliquots were stored long term at –20 °C.

M13K07 Virus (M13 virus) was obtained from the Vanderbilt Molecular Recognition and Screening facility in a stock concentration of 3.3×10^{11} virions/ml and was diluted in phosphate buffered saline containing 0.1 % tween-20 (PBS-T) to working concentrations immediately prior to experiments.

Antibody Immobilization on Filament

120 μm diameter clear polyester filament (440 yd spool, Sulky Invisible, Punta Gorda, FL) was obtained from webofthread.com (Kenmore, WA). Glass, polyethylene, polyester, nylon, PVDF, and silk filaments were tested and rated based on autofluorescence at common wavelengths, flexibility, chemical composition, and strength. The polyester filament provided the best combination of strength and flexibility and exhibited less intrinsic autofluorescence than the other polymer filaments. In addition, polyester provided an excellent substrate upon which to passively adsorb antibodies. The filament was wound around the ends of a PhastGel sample applicator (Amersham Biosciences) and placed within the concave teeth as shown in Figure 2. Combs were cleaned with a nearly saturated solution of NaOH in approximately 60% ethanol prior to winding the filament. The comb/filament apparatus was washed in 70% ethanol, rinsed, washed in 10% HCl, and rinsed again.

The filament was allowed to dry completely, and 0.75 μl of antibody solution was applied to each tooth of the comb.

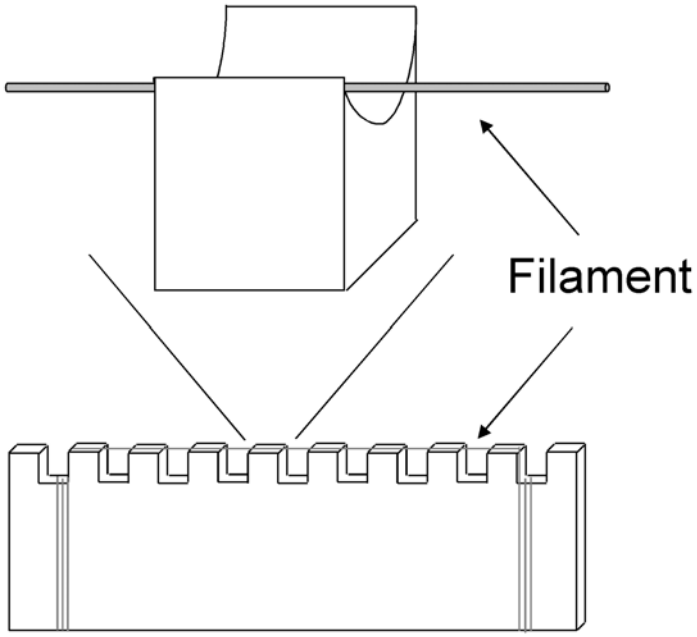

Figure 2: Filament was wrapped around the ends of a gel loading comb and then placed across the concave teeth for antibody spotting.

In some assays, a low concentration of cytochrome C labeled with Cy3 protein label was added to the antibody solution (~2 μg/μl) as an indicator of antibody distribution. The comb and filament were incubated in a humidified box for 45-60 minutes to allow time for adequate adsorption of antibody to the filament. Following incubation, the comb and filament were immediately rinsed in PBS containing 0.1% tween-20 (PBS-T) to remove unbound antibody from the filament. Filaments were used within two hours of this final rinse.

Automated Virus Detection In Microcapillary Chambers

A rotary stage and control system from Yaskawa (Waukegan, IL) were used to control the movement of the filament through five processing chambers. The system of micro-reaction chambers was attached to the top of a horizontal stage using Lego™ building blocks. This simple modular design allowed chambers to be easily repositioned or replaced. Three sets of chambers were placed in parallel onto the horizontal stage. After each filament was threaded through the chambers, they were attached to a single rotating spindle on one end and small weights on the other. In this manner, three filaments could be controlled in parallel with each other using a single interface. The rotary stage was controlled through a LabView Virtual Instrument (National Instruments, Austin, TX) that wound and unwound the filament to maneuver the probe segments sequentially through each chamber as depicted in Figure 3.

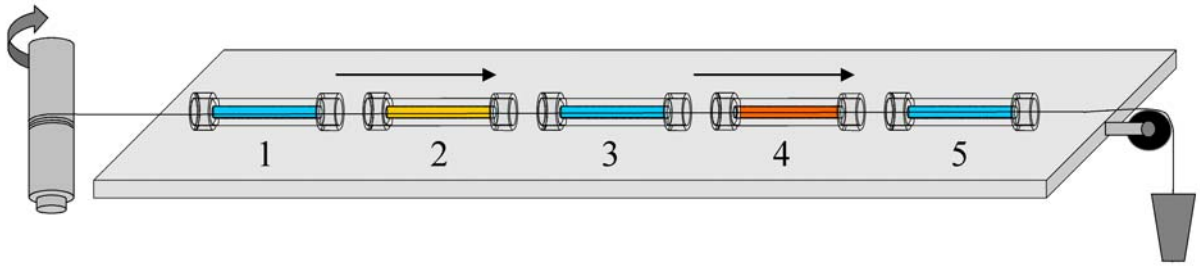

Figure 3: Capillary reaction chambers were arranged sequentially on a horizontal stage. A filament with antibody segments immobilized at known locations was threaded through the chambers. One end was attached to the shaft of a precision rotary stage, and a small fishing weight was attached to the other. The rotary stage controlled the movement of the antibody segments through each reaction chamber by winding and unwinding the filament.

The LabView interface controlled the speed of the filament through the chambers, oscillatory movements within the chambers, and total residence time within each chamber. Filaments were oscillated 2 cm at a velocity of 0.5 cm/sec for the requisite time within each chamber before moving to the next. Overall travel of the filament from the first chamber through the final was approximately 40 cm. Table 1 summarizes the contents and purpose of each chamber. Chambers are separated by a distance of 1 cm, but contamination between chambers is a possibility. Cross-contamination between microcapillary chambers was tested by placing labeled anti-M13 in one chamber followed by a chamber containing only PBS-T. Mock processing was performed using typical filament motion parameters, and solutions from each capillary were collected and spotted onto glass slides for fluorescence scanning.

To test for the consistency of virus detection, filaments were prepared with four distinct anti-M13 segments as described above. The specificity of virus detection was tested by adding negative control segments to each filament. Filaments were prepared with an alternating pattern of anti-M13 and anti-E that was not specific for M13 virus, for a total of four segments on each filament. Labeled cytochrome C was not used as a positive control marker in these assays. Reaction conditions for both experiments are summarized in Table 2. To test the diffusion dependence of this system, virus incubation time was varied to examine the dependence of virus detection on antigen diffusion. Filaments were prepared with a negative control anti-E tag segment adjacent to five anti-M13 segments. Cy3-labeled cytochrome C was added to the spotting solution prior to filament preparation for a final concentration of approximately 2 μg/ml, serving as a positive control, so that spotted regions could easily be determined after scanning.

Table 1: Contents and purpose of each reaction chamber.

	Solution	Purpose
Chamber 1	PBS-T	Rehydrate probes, block non-specific binding
Chamber 2	M13 virus	Expose immobilized antibody to antigen
Chamber 3	PBS-T	Wash away unbound antigen
Chamber 4	Labeled anti-M13 antibody	Expose bound virus to labeled antibody
Chamber 5	PBS-T	Wash away unbound labeled antibody

Virus incubation time course experiments were done statically, and filaments were not oscillated within the virus chamber, but oscillation within other chambers was similar to previous experiments. Table 2 summarizes the other reaction parameters for this assay. The effect of filament oscillation on virus detection was also tested. A negative control segment was adjacent to four anti-M13 segments on each filament. One set of filaments was oscillated within the virus chamber similar to previous experiments, while a second set was incubated using static conditions. Additional reaction conditions are summarized in Table 2.

The sensitivity of virus detection was tested using larger capillary reaction chambers (1 mm ID, 60 μl). In these experiments, filaments had a negative control segment adjacent to four anti-M13 segments. Segments were incubated with 1.7×10^6, 1.7×10^7, 1.7×10^8, 1.7×10^9, or 1.7×10^{10} virus particles in 60 μl PBS-T for 100 minutes. The number of virus particles used in these experiments corresponded to the number of particles that was found to be detectable using plate ELISA. The total assay time of 175 minutes was 45 minutes less than the equivalent ELISA time. Table 2 summarizes the other reaction conditions.

ELISA

A standard criss-cross serial dilution analysis was performed to determine the optimal concentrations of immobilized capture antibody and detecting antibody (anti-M13 conjugated to HRP) that yielded the highest sensitivity to virus. 50 μl of PBS was added to each well of a 96 well ELISA plate.

Table 2: Summary of reaction parameters used in each experiment.

	Experiment				
	Consistency of virus detection	Specificity of virus detection	Diffusion Dependence	Effects of Filament Oscillation	Detection Sensitivity
Chamber 1	10-15 min	10-15 min	10-15 min	10-15 min	10-15 min
Chamber 2	35 min	45 min	25-990 min	45 min	100 min
Chamber 3	5 min	5 min	5 min	5 min	5 min
Chamber 4	35 min	45 min	45 min	45 min	50 min
Chamber 5	10 min	10 min	10 min	10 min	10 min
Oscillation	2 cm, 0.5 cm/sec	2 cm, 0.5 cm/sec	None in virus chamber	2 cm, 0.5 cm/sec	2 cm, 0.5 cm/sec
Chamber Volume	25 μl	25 μl	25 μl	25 μl	60 μl
Virus Particles	8.3×10^8	8.3×10^8	8.3×10^8	8.3×10^8	1.7×10^7 – 1.7×10^9
Labeled Antibody	40-50 μg/ml AF555 anti-M13	40-50 μg/ml AF555 anti-M13	40-50 μg/ml AF647 anti-M13	40-50 μg/ml AF647 anti-M13	40-50 μg/ml AF647 anti-M13

Next, 50 μl of unlabeled anti-M13 (50 μg/ml in PBS) was pipetted into column 1 and serially diluted 1:2 through column 11, leaving column 12 with only PBS. The plate was incubated for 1 hour at room temperature in a humidified box, rinsed 3 times with PBS-T, and blocked with 50 μl PBS-T for 15 minutes. After blocking, 50 μl of virus solution (3.3×10^{10} virions/ml) was added to each well, and the plate was incubated for another hour in a humidified box, followed by 6 rinses with PBS-T. 50 μl PBS-T was added again to each well of the plate. HRP-conjugated anti-M13 was diluted 1:500 in PBS-T, and 50 μl was added to each well in the first row of the plate. The antibody was then serially diluted 1:2 through row G, leaving row H with PBS-T only. The plate was then incubated for 1 hour in a humidified box and rinsed. To develop the plate, 50 μl of the HRP substrate (50 mM sodium citrate buffer, pH4.2, containing 90 mM ABTS and 0.05 mM H_2O_2) was added to each well and left at room temperature. Absorbance readings were taken using a microplate reader (405 nm) at both 20 minutes and 75 minutes, and the signal to noise ratios were calculated by dividing the raw values with the corresponding negative control values in column 12. Optimal concentrations for capture antibody and HRP-conjugated detecting antibody were found to be 1.56 μg/ml and 1:2000 dilution, respectively.

ELISA experiments using the optimized values for primary and detecting antibody were performed to determine the sensitivity of this assay to M13 virus. The ELISA plates were processed as described above. Additional wells containing virus of each concentration were added in duplicate into the wells of column 7 for use as negative controls. Signal to noise ratios were determined as described above.

Reagent Testing

Preliminary experiments and optimization of immobilized antibody were performed using antibody-filament reactions in 2 ml Eppendorf tubes in place of capillary reaction chambers. After blocking in PBS-T for 10 minutes, the filaments were transferred to a virus solution ($3.3x10^{10}$ virions/ml) and gently rocked on an orbital shaker for 30 minutes. After a 5 minute wash in PBS-T, the filaments were again removed and placed in a solution of anti-M13 labeled with either Alexa Fluor 647 or Alexa Fluor 555 protein label (~10 μg/ml in PBS-T) and were gently rocked for an additional 30 minutes. After a final wash of 10 minutes in PBS-T, the filaments were scanned for fluorescence. Due to the relatively large volume used for Eppendorf processing, the amount of virus used was approximately 50 times greater than automated, capillary chamber experiments.

Detection and Analysis

Following all experiments, filaments were removed after the final wash, taped to glass microscope slides, and scanned in a GenePix 4000B microarray scanner (Axon Instruments, Union City, CA). Due to the three dimensionality of the filament, a series of scans on a single filament was obtained at different focal depths to determine the scan depth for maximum fluorescence. A 75 μm depth of focus yielded the strongest signal, so all subsequent filaments were scanned at this depth. Filaments were scanned using both the 532 nm and 635 nm wavelengths of the scanner, and segment fluorescence and background fluorescence were quantified (Image Pro 4.0, Media Cybernetics, San Diego, CA) by taking the average pixel fluorescence over the segment area. Fluorescence images from the microarray scanner were artificially rendered green or red by the

scanning software to better distinguish the 532 nm and 635 nm wavelengths of the device. To determine the signal to noise ratio of each experiment, fluorescence of anti-M13 segments was divided by the background fluorescence or negative control fluorescence if a negative control was present. Analysis of variance of fluorescence signals and background signals was used to determine statistical significance ($p<0.05$).

Results

Figure 4 shows a typical fluorescence pattern after detection of M13 virus during reagent testing experiments. This experiment shows little or no detectable cross reactivity between M13 virus and a non-specific anti-E antibody. Immobilized segments one and two (left side of Figure 4) are each labeled with a different fluorescent tag and serve as positive controls for each wavelength. These segments should fluoresce at their corresponding wavelengths under all conditions. Segment three is an anti-E tag monoclonal antibody that is not specific for M13 virus and serves as a negative control. This region should not bind virus or detecting antibody and, therefore, should not fluoresce under any conditions. Segments four, five, and six contain unlabeled M13 Ab and should fluoresce only if virus is present. Holding all other parameters constant, filament oscillation within the virus chamber was also tested to determine whether it increases segment fluorescence over a static virus incubation.

Using a static incubation, the average signal to noise ratio for each of three filaments (each with four segments) is 1.4, 1.2, and 2.0 (avg = 1.5). Filament oscillation increased the average signal to noise ratio nearly 5 times to 5.6, 6.6, and 8.8 (avg = 7.0). After subtracting intrinsic fluorescence of the filament at the appropriate wavelengths

from all spotted regions, signal to noise was defined as the average fluorescent signal of anti-M13 regions divided by average fluorescence of negative control regions. When a negative control was not present, signal to background was used to judge the success of the experiment. In these circumstances, average fluorescent signal of anti-M13 regions was divided by average fluorescence of empty regions on the filament that were processed in the same manner as the anti-M13 regions. These experiments suggest that filament oscillation leads to an increase in virus interaction with the filament-bound antibody.

After appropriate reaction conditions were identified, the effectiveness of automated filament movement through microcapillary chambers was evaluated. To determine detection repeatability, four filaments each with four immobilized anti-M13 segments were prepared, threaded through the system of capillary chambers, and filament motion was programmed into the LabView virtual instrument. The top panel in Figure 5 shows both the fluorescence pattern obtained from the filament scan of one filament and the average segment fluorescence of each segment. Comparison of four filaments, each with four segments, yielded an overall average for all sixteen segments of 10542 ± 1374 (mean ± SD) and an overall coefficient of variation (CV) of 0.13. Intra-assay CV for individual filaments varied from 0.05 to 0.4.

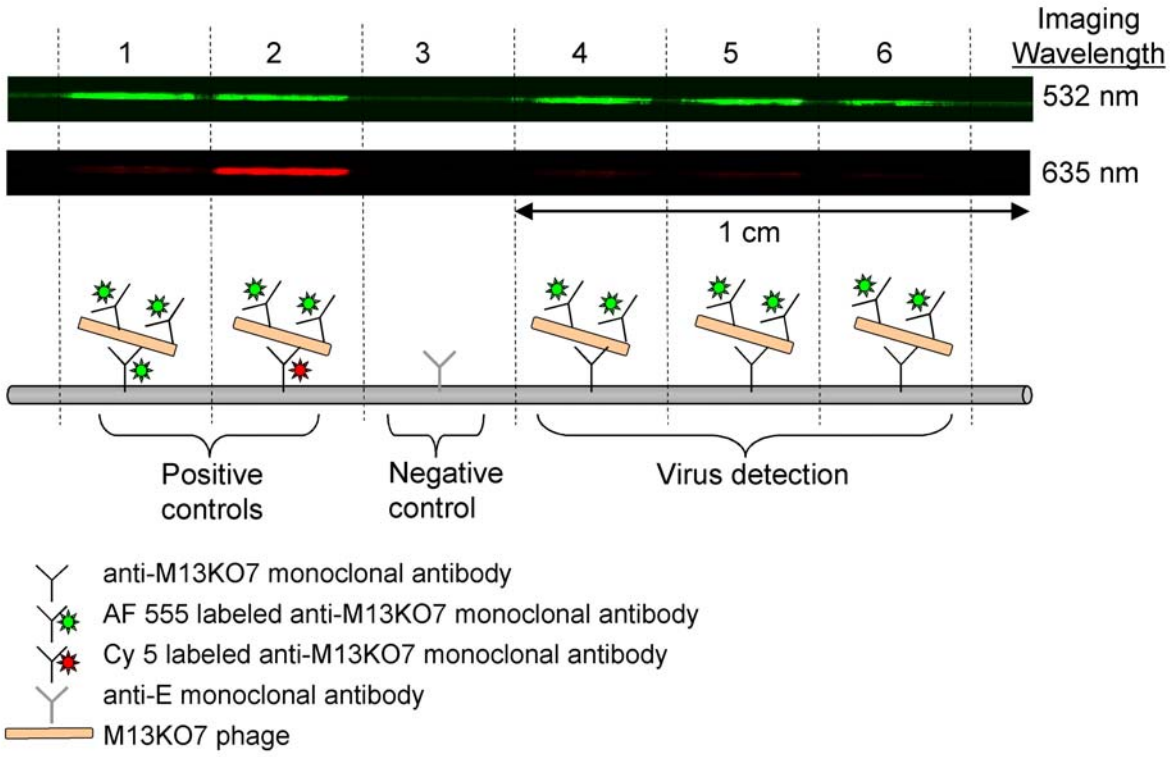

Figure 4: Immobilized anti-M13 detects the presence of M13 virus in solution. Segments 1 and 2 are fluorescently labeled positive controls and segment 3 shows the level of cross-reactivity with a non-specific negative control antibody. Segments 4-6 show virus detection in solution.

Detection specificity was also evaluated. For these experiments, three filaments were prepared with patterns of four alternating segments of unlabeled anti-M13 and unlabeled anti-E as a negative control. The bottom panel in Figure 5 shows the florescence pattern and the average segment intensities from one of these experiments. In this experiment, signal from anti-M13 segments is approximately 40 times greater than the negative control anti-E segments. The overall average results from all three filaments in this set were ~30 times greater for anti-M13 segments (16264 ± 5396) than negative control segments (573 ± 278). Overall CV for anti-M13 and negative control signals was 0.33 and 0.48, respectively. Intra-assay CV calculations were not possible since only two segments of each type were present on each filament. A direct fluorescence comparison between reproducibility and specificity graphs is not possible since all parameters were not the same for each test. These experiments provide strong evidence that this system consistently and specifically detects virus in solution with a high signal to noise ratio compared to a non-specific antibody.

Since immobilized antibody concentration significantly effects sensitivity of standard ELISA, an experiment was performed to determine the optimal spotting concentration of anti-M13 for the filament based system. Anti-M13 of varying concentrations was spotted and immobilized on a filament and then processed through capillary reaction chambers to determine which concentration gave the strongest signal. A negative control anti-E segment was adjacent to increasing concentrations of anti-M13 spotting solution, and the filament was processed through capillary reaction chambers using parameters similar to previous virus detection experiments.

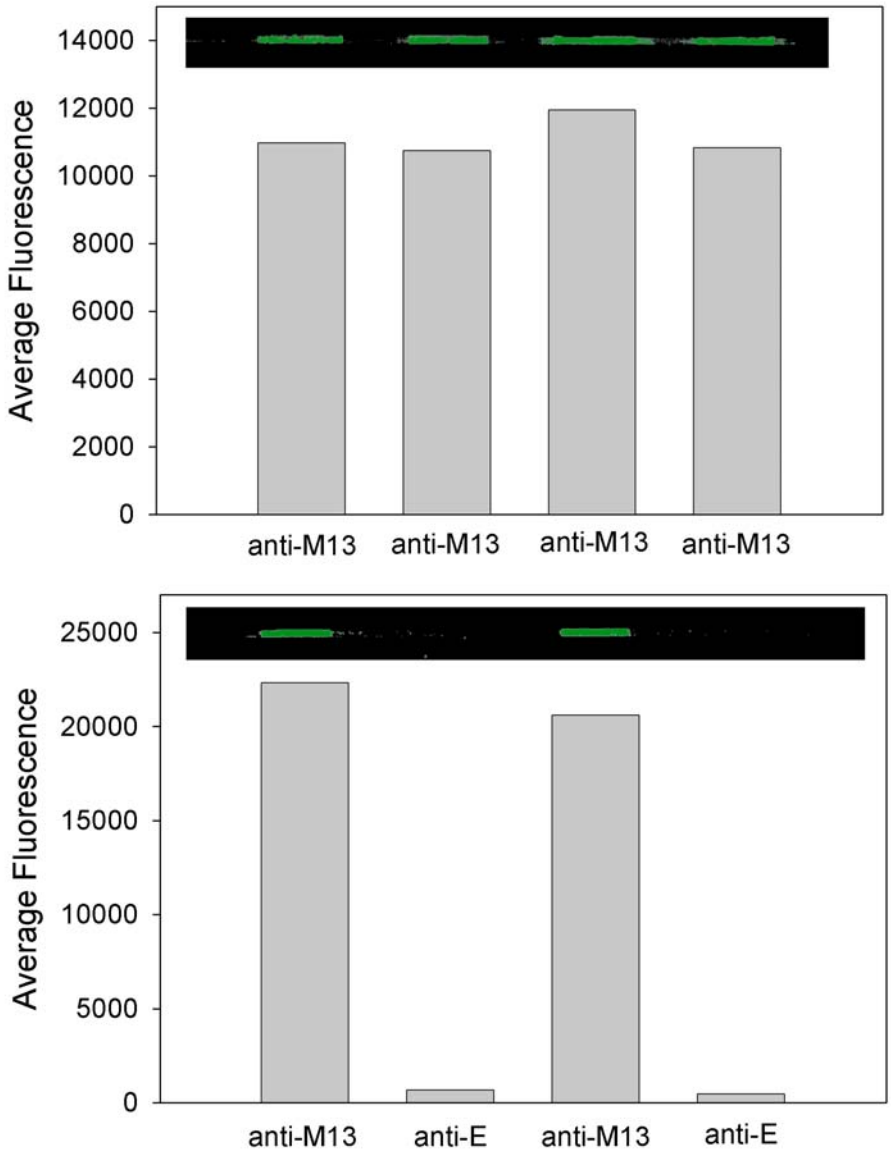

Figure 5: Typical fluorescence patterns and average fluorescence of immobilized probe segments, showing repeatability (top) and specificity (bottom). Fluorescence varies by approximately 5% between segments (top), and fluorescence from anti-M13 segments is approximately 40 times greater than negative control anti-E segments (bottom).

As Figure 6 illustrates, the data shows an increase in signal intensity up to 600 μg/ml, after which the signal begins to drop, a trend that is consistent with the literature for antibodies immobilized on other polymers (25).

Antigen-antibody sensitivity was determined using a traditional ELISA. Three ELISAs were run to determine the lower limit of detection of M13 virus with anti-M13 antibody. The number of virus particles ranged from 1.7×10^4 to 1.7×10^9, and each assay included 8 trials for each condition. The lowest number of virus particles that yielded a statistically significant signal was 1.7×10^7 ($p<0.05$) (Figure 7). Experiments were performed to determine the lower limit of sensitivity of this filament-antibody recognition assay (FARA) approach. Five filaments, each containing four distinct M13 Ab segments and one negative control anti-E segment, were incubated with five different virus copy numbers comparable to virus numbers detected with standard ELISA. Incubation times for virus and detecting antibody were 100 min and 50 min, respectively, so that total assay time for automated filament based detection (~175 minutes) was 20% less than the ELISA (~220 min). These approximate assay times include all washing steps and ELISA developing time but do not include filament or ELISA preparation time. As shown in Figure 7, the filament based assay detected similar amounts of virus with similar signal to noise ratios as standard ELISA. Diffusion of the virus to the filament surface may be a major factor that limits detection sensitivity with the FARA approach. Figure 8 shows results from a time course of virus incubation time. Fluorescence intensity increases with virus incubation time, which is consistent with the hypothesis that diffusion/delivery of virus is an important factor. However, our data suggests that other factors contribute as well, since signal intensity is not proportional to

the square root of the incubation time. Nevertheless, virus incubation time appears to be a critical parameter.

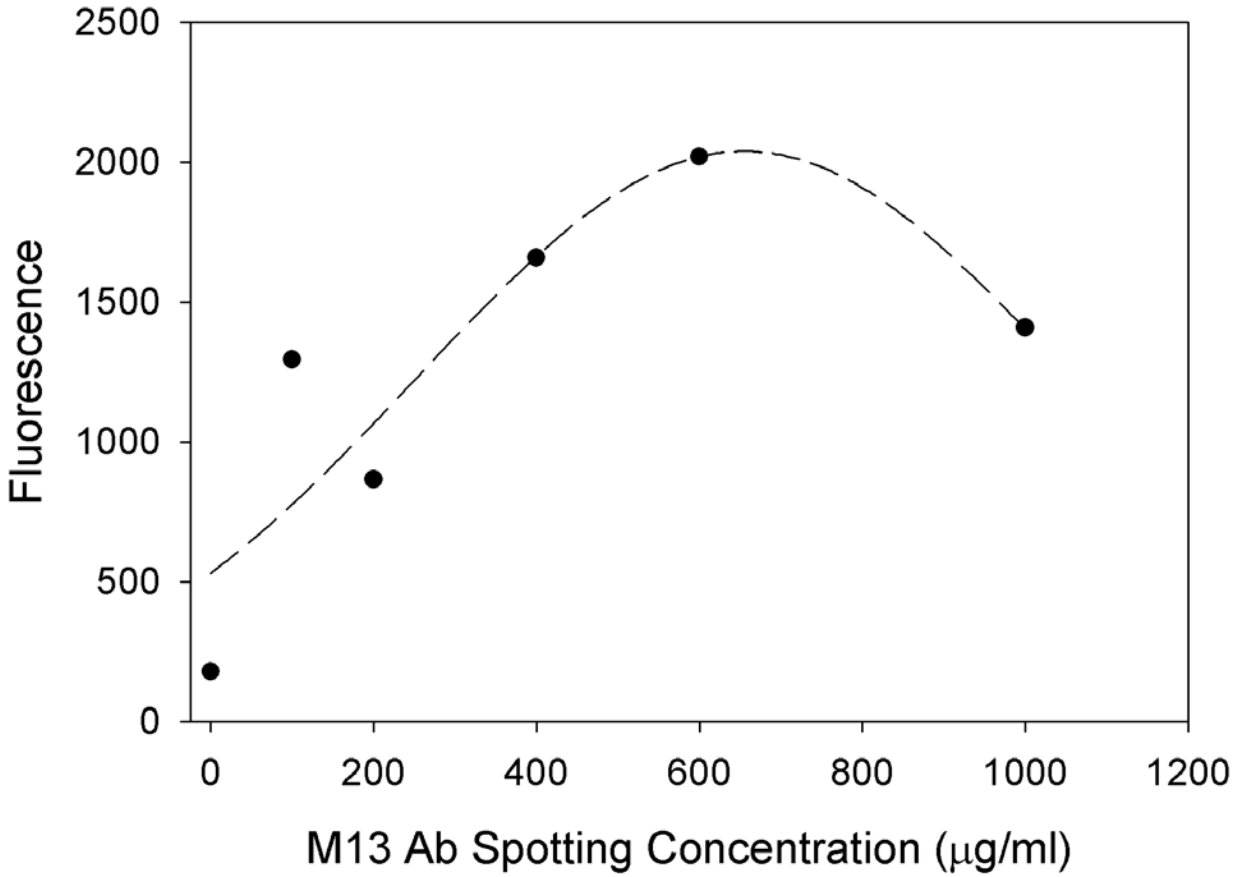

Figure 6: Fluorescence intensity increases with spotting solution concentration up to about 500 μg/ml. At concentrations above this point, intensity begins to decrease.

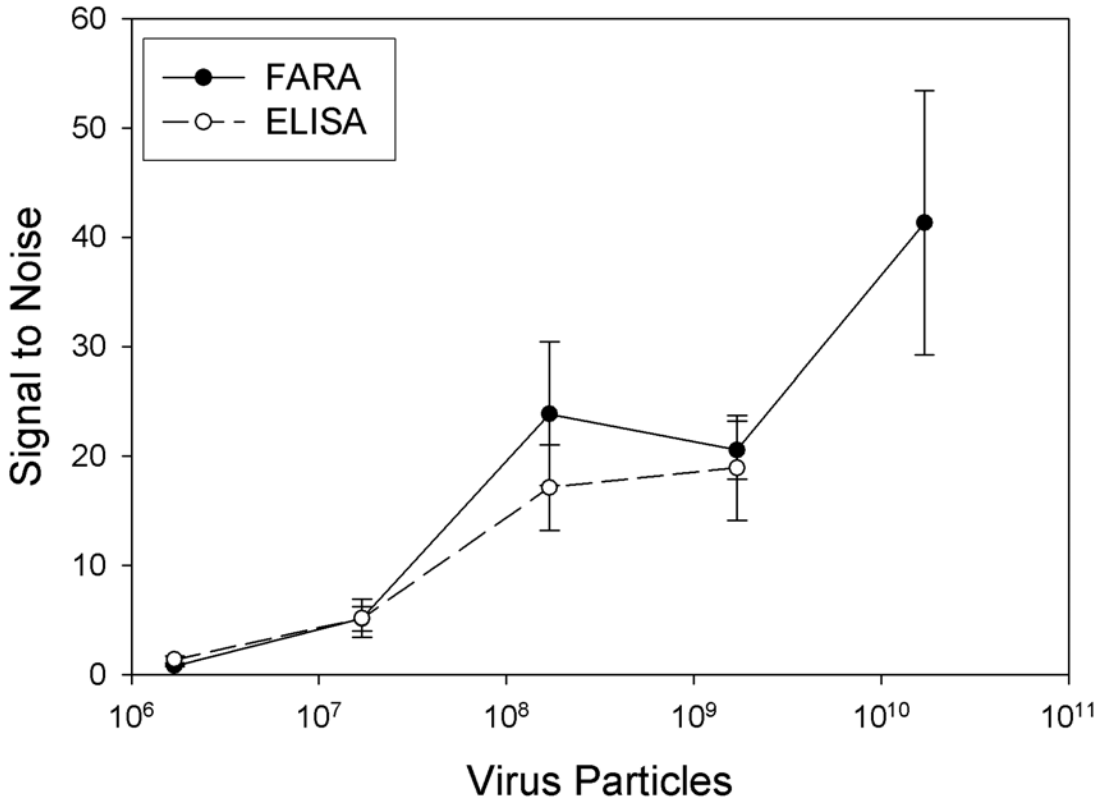

Figure 7: Detection and calibration curve for both FARA (closed circles) and ELISA (open circles). Both methods have a lower limit of sensitivity of ~1.7 x 10^7 virus particles. Data points represent SNR obtained for different virus copy numbers (mean ± SD, n=3 experiments for ELISA and 4 spotted regions for FARA); *indicates significantly increased signal over negative controls

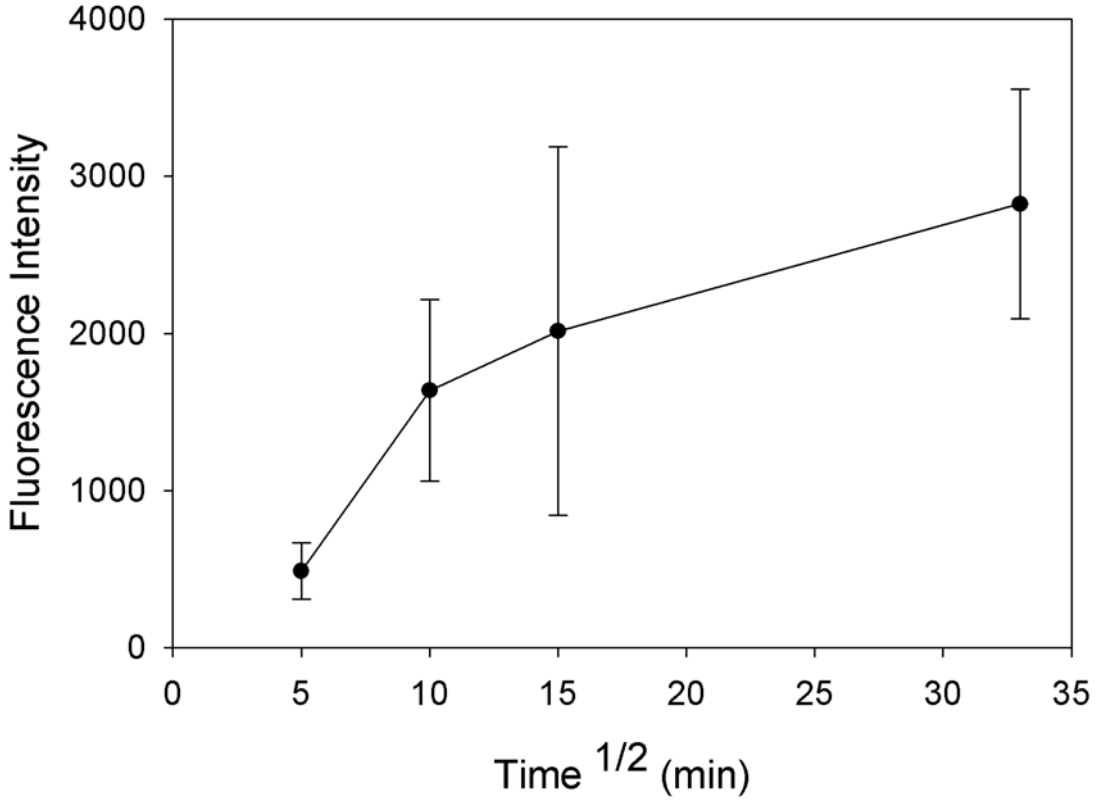

Figure 8: Signal strength increases with virus incubation time (mean ± SD, n=3).

Discussion

These data demonstrate that anti-M13 antibody can be passively adsorbed to a polyester filament, and the antibody remains functional. Direct binding is shown by the hydrophobic attachment of fluorescently-labeled control antibody (Figure 4). Indirect evidence suggests that binding sites on filament-immobilized antibodies remain active and capture virus out of solution (Figure 4, Figure 5, Figure 6, Figure 7, Figure 8). The addition of tween-20 to the wash solution after initial capture antibody attachment appears to effectively block further non-specific filament-antibody interaction. This is supported by the observation that the fluorescently-labeled second antibody does not directly interact with the filament, as shown by the non-fluorescent regions between immobilized segments.

The lower limit of sensitivity of this assay was similar to a traditional plate ELISA. The limit of sensitivity of the FARA approach is 1.7×10^7 particles (~400 pg), which is similar to the limit of traditional ELISA (Figure 7). This level of sensitivity was achieved in a shorter assay without the required amplification step for ELISA and with automation of the reaction process. The detection area for one spot using the FARA approach is approximately 7.5×10^5 μm^2 (d=120 μm, l=2000 μm) FARA detects 1.7×10^7 particles, which means that at the lower limit of sensitivity, FARA detects 22.5 virus particles/μm^2. A similar calculation shows that a single well in an ELISA with a much larger detection area of approximately 3.8×10^6 μm^2 (d=0.7 cm) has a detection sensitivity of only 0.44 virus particles/μm^2. Using this measure, FARA is approximately 50 times more sensitive per unit area than ELISA.

Exact calculation of mass transfer coefficients for each system can not be made, but the ratio of the coefficients can be estimated by making some assumptions. The total amount of virus transferred per unit time can be calculated by multiplying the mass transfer coefficient (k), the detector surface area (A), and the virus concentration (C). The total amount of virus transferred can be calculated by multiplying the product kAC by the total virus incubation time (T). From Figure 6, both assays produced similar signal to noise ratios using 10^7 to 10^8 virus particles. If the assumption is made that equal numbers of virus particles are transferred to the surface within this range of virus particles, the ratio of the mass transfer coefficients is estimated as: $k_F/k_E = c_E A_E T_E / c_F A_F T_F$, where the subscripts E and F denote ELISA and FARA. Since concentration, area, and assay times are known values, this ratio is approximately 3. Several assumptions were made in this calculation that need to be further verified.

Although FARA sensitivity is similar to ELISA, adding an amplification step may increase sensitivity even further. Precipitating substrates used in ELISA may be an attractive amplification method in this system, as well, but it is not clear whether the precipitant could be confined to each spotted region as filament processing continued. If precipitants became dissociated from specific regions, detection of individual regions would not be possible.

The microcapillary geometry of the FARA approach may account for the high sensitivity observed. The linear geometry of the microcapillary chambers combined with filament motion reduces the diffusion distance required for target molecules to encounter immobilized probes. In this system, probes can be slowly oscillated within a reaction chamber, allowing the immobilized probes to query the entire axial length of target

solution. As a result, the limiting diffusion distance is the radial distance from the filament to the edge of the chamber. The current size of the capillary chambers is approximately 700 or 1000 μm ID. Since the filament diameter is 120 μm, the radial diffusion distance is either 290 μm or 440 μm, which is an order of magnitude less than the diameter of a 96-well ELISA plate. Based on values reported in the literature for large proteins, the virus diffusion coefficient was estimated to be on the order of 10^{-8} cm^2/sec (20,21). Assuming the simple diffusion relationship of $d = \sqrt{2Dt}$, diffusion of 290 μm would still take nearly 700 min. Much smaller capillaries are available that could reduce this distance to well under 100 μm, a distance over which diffusion could occur much more quickly. Although this distance is still too great for target molecules to completely diffuse under reasonable incubation times, it is much smaller than the distance required in a plate based assay.

A possible complication arising from the filament motion and open geometry of the capillary reaction chambers is fluid contamination between chambers. However, cross-contamination experiments showed that contamination is minimal and is less than 4% between chambers. The addition of extra wash chambers is an easy solution, which could be used to further reduce carry over between adjacent chambers.

CHAPTER IV

ADAPTIVE VIRUS DETECTION USING FILAMENT-COUPLED ANTIBODIES

Gregory P. Stone
Kelvin S. Lin
Frederick R. Haselton

Biomedical Engineering
Vanderbilt University
Nashville, Tennessee

(This manuscript was submitted for review to *Journal of Biomedical Optics*)

Abstract

We recently reported the development of a filament-antibody recognition assay (FARA)(43) which, through the use of antibodies coupled to a moveable filament, detects the presence of virions by building an ELISA-like antibody-antigen sandwich attached to a filament. In this report, we combine the motion of the filament with a fixed laser-based optical detector to enable real-time controlled detection of virions in solution. A 638 nm laser with a photomultiplier at a right angle provided continuous monitoring for the presence of the anti-M13 monoclonal IgG_{2a} labeled with Alexa Fluor 647. Entrainment of this labeled antibody was indicative of virus captured by unlabeled anti-M13 previously coupled at known locations along the filament. As expected, as virus incubation time increased, lower concentrations of virus were detectable. A one-minute incubation was required to detect 10^{10} virions and 40 minutes was required to detect 10^{8} virions. Since fluorescence intensity is measured in real-time, this information can be used to position the filament. Therefore, an unknown virus sample can be subjected to both a rapid initial test and then, if necessary, a slow follow-up high sensitivity test. In tests of the feasibility of this approach, a thirty minute virus (3.3×10^{10} virions/ml) incubation time followed by recycling the captured virus to the detecting antibody chamber (20 μg/ml) found an increase in signal roughly proportional to the 0.5, 1, and 2 minute residence times in the detecting antibody chamber. Tests of recycling capture antibody regions to the virus chamber (3.3×10^{10} virions/ml) for cumulative virus incubation times of 1, 5, or 10 minutes followed by an additional 1 minute detecting antibody (20 μg/ml) incubation also found an increase in signal proportional to the virus

incubation time. Filament positioning combined with on-line optical detection provides new flexibilities for developing adaptive molecular recognition assays.

Introduction

The need for fast, reliable, and cost effective pathogen detection is increasing as a result of both increasing health care costs and the rising threat of bioterrorism. Traditional methods, which can often be completed using existing laboratory infrastructure and equipment, are still the most reliable and robust techniques and can used to detect a broad range of pathogens. However, these techniques require highly trained laboratory personnel and can be both labor and time intensive. Since these methods typically involve growth of the organism in culture or infection of a virus in a suitable host, these techniques may require days before identification of the hazard is complete (34,44).

Immunological methods have been developed that encompass a very broad range of applications such as the detection of bacterial cells, spores, viruses, proteins, or any other toxin that elicits an immune response (34,44,45). Numerous new immunological detection strategies have been reported in the literature, and several reviews have been written summarizing the state of the art of immunological biosensors (34,46,47). Several of these methods are based upon changes in electrical properties as antigen binds to an antibody coated substrate (36,37,47-49). Many others have been reported that incorporate optical detection of bound antigen. For example, evanescent waves have been used to excite bound antigen on a fiber optic waveguide using a fluorescently labeled detecting antibody. Ligler *et al.*, have extended this technique to incorporate a two dimensional waveguide upon which an entire array of probe molecules has been immobilized (40-42). However, many of these assays require complex microfluidics, and automation of fluid handling and processing is very difficult to incorporate into these

systems. In addition, these optical techniques usually lack a feedback mechanism to determine when the experimental signal has reached an adequate level. Rather, these assays must be run to completion in order to ensure sufficient signal, wasting time, reagents, and sample.

We have recently reported the development of a filament-antibody recognition assay (FARA). In this report, we incorporate an integrated optical detection method to enable optical feedback control of virus detection. FARA is a sandwich-based immunoassay in which antibodies are immobilized on the surface of a monofilament rather than on a polystyrene plate. Using a rotary stage to control filament position, each antibody bearing region is passed through a series of five fixed reaction chambers (Figure 9). The first chamber washes excess antibody from the filament uses a non-ionic detergent to block non-specific binding in subsequent steps. Antibody regions are exposed to the unknown virus solution in the second chamber and bind virus out of solution, if the corresponding virus is present. After a brief wash in the third chamber, the antibody regions are exposed to a fluorescently-labeled detecting antibody that will bind to virus on the filament that has previously been captured from solution. Following a final wash to remove any unbound reagents, the antibody regions on the filament are passed through an integrated detector where the fluorescently-labeled detecting antibody is excited with a diode laser. Fluorescence from the detecting antibody is detected by a photomultiplier, and the signal values are used to determine if additional testing or further processing is required.

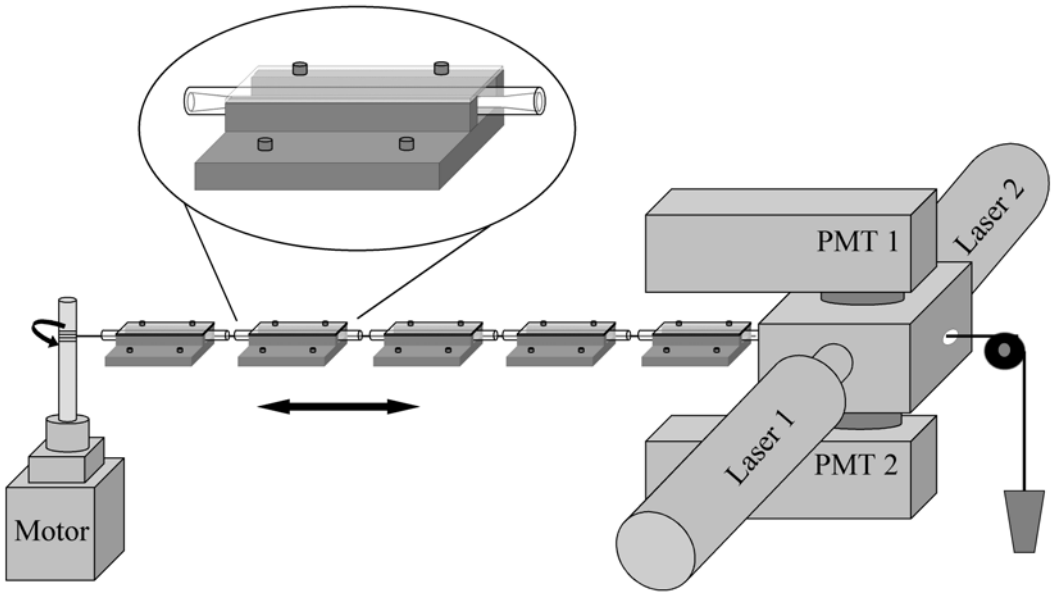

Figure 9: Filament-coupled antibodies are pulled through a series of five reaction chambers before passing through a fluorescence detector. Detection of filament-bound virus is achieved through a fluorescently-labeled detecting antibody that is excited with a diode laser. Fluorescence is detected by two photomultiplier tubes.

Materials and Methods

Antibody and Virus reagents

M13K07 phage and anti-M13 monoclonal antibody provide a suitable model system for this design, but nearly any antibody/antigen system would be suitable for this approach. However, M13K07 is a harmless phage that is well characterized, so assays can be performed with minimal safety concerns. M13K07 Virus (M13) was obtained from the Vanderbilt Molecular Recognition and Screening facility in a stock concentration of 3.3×10^{11} virions/ml and was diluted in phosphate buffered saline containing 0.1 % tween-20 (PBS-T) to working concentrations immediately prior to experiments. Anti-M13 monoclonal IgG_{2a} (anti-M13) and anti-E tag monoclonal IgG_{2a} (anti-E) were obtained from Amersham Biosciences (Piscataway, NJ) and fluorescently labeled with Alexa Fluor 647 (AF647, Molecular Probes, Eugene, OR). Labeling procedures were performed according to the manufacturers' instructions. The concentration of the labeled antibody along with the degree of labeling was calculated from the absorbance at 280 nm and the peak label absorbance. Aliquots were stored long term at –20 °C, and working solutions of both labeled and unlabeled antibody were stored at 4°C.

Antibody Immobilization on Filament

Antibodies were passively adsorbed to a clear polyester filament with a diameter of 120 μm (Sulky Invisible, Punta Gorda, FL). The filament was wound around the ends of a PhastGel sample applicator (Amersham Biosciences) and placed within the concave teeth as described previously (43). The comb/filament apparatus was washed in 70%

ethanol, rinsed, washed in 10% HCl, and rinsed again. The filament was allowed to dry completely, and 0.75 μl of capture antibody solution (500 μg/mL) was applied to each tooth of the comb. To allow time for adequate adsorption of the capture antibody to the filament, the comb and filament were incubated in a humidified box for 45 minutes. Following incubation, the comb and filament were immediately rinsed in PBS containing 0.1% tween-20 (PBS-T) to remove unbound capture antibody from the filament. Filaments were used within one hour of the final rinse.

Filament Processing

One-quarter inch (OD) thick-walled glass capillary tubing was cut into 75 mm lengths, and the ends were flared outward to facilitate smooth movement of the filament in and out of the chambers. Table 3 summarizes the contents and function of each chamber. Each glass chamber was housed in an aluminum holder with holes for two positioning bolts as shown in the inset of Figure 9**.** A horizontal aluminum stage with a matrix of predrilled holes allowed the chambers and holders to be easily aligned and fastened. After a filament was threaded through the chambers and detector, it was attached to a rotating spindle atop a rotary stage on one end and a small weight on the other as shown in Figure 9.

Table 3: Contents and description of each chamber.

Chamber	ID (mm)	Solution	Function
1	2	PBS-T	Rehydrate probes, block non-specific binding
2	0.75	M13 virus	Expose immobilized antibody to antigen
3	2	PBS-T	Wash away unbound antigen
4	0.75	Labeled anti-M13 antibody	Expose bound virus to labeled antibody
5	2	PBS-T	Wash away unbound labeled antibody

Filament movement through the five chambers and detector was performed using the rotary stage and control system from Yaskawa (Waukegan, IL). The rotary stage was controlled through a LabView Virtual Instrument (National Instruments, Austin, TX) that wound and unwound the filament to position the probe segments sequentially through each chamber. The LabView interface controlled the speed of the filament through the chambers, oscillatory movements within the chambers, and total residence time within each chamber. Filaments were oscillated 2 cm at a velocity of 1 cm/sec for the requisite time within each chamber before moving to the next. Overall travel of the filament from the first chamber through the detector was approximately 50 cm.

Fluorescence Detection

A laser excitation source was used to excite a fluorescently labeled detecting antibody specific for the bound M13 virus. The detection system incorporated two diode lasers at a 90° orientation to the filament. The dual laser design allowed for flexibility when choosing appropriate fluorescent labels for detection. The filament ran through a detection chamber (Newport-Oriel, Stratford, CT) that allowed easy coupling of two lasers and two PMTs. Figure 9 shows a diagram of the virus detection scheme. Laser 1 was a 25 mW, 638 nm diode laser (Coherent, Santa Clara, CA) and was used to excite the AF647 fluorescent dye. Laser 2 was a 532 nm, 20 mW diode-pumped, solid state laser (B&W Tek, Inc., Newark, DE) that was used to excite AF555 fluorescent dye, which was used primarily in preliminary experiments. The detector's dual laser and dual PMT design allows for two fluorescent labels to be used concurrently, adding flexibility to this technique. The lasers were attached to the detection chamber on either side using custom

adaptors to fit the ports of the chamber. A polarizer was placed within the adaptor to reduce the 638 nm laser power to approximately 5 mW.

The PMTs were also attached via custom adaptors to the top and bottom of the chamber. Reflectance of the laser light from the filament was a significant issue, so choice of emission filters was critical to achieving a high signal to noise ratio (SNR). For the AF647 channel, long pass filters with cutoffs at 685 nm (Chroma, Rockingham, VT) and 665 nm (Melles Griot, Rochester, NY) were combined to filter out reflected laser light. The AF555 channel combined a bandpass filter centered at 565 nm (30 nm bandwidth, Chroma) with a long pass filter (570 nm cutoff, Melles Griot) to filter out reflected light. Filters were placed in between the sample chamber and the PMTs as in Figure 10.

Figure 10 shows the optical path for our detector. A custom metal slit was fashioned out of brass and placed in the laser path, to minimize the area on the filament illuminated by the laser. After exciting bound detecting antibody, fluorescence emission from the detecting antibody passes through a pinhole that reduces much of the reflected laser light. The light then passes through a pair of emission filters, which removes the excitation light, while allowing fluorescence to pass through to the PMT (R928, Hamamatsu). Each PMT was powered by an 800 V signal and the resulting current was converted to voltage and amplified by a factor of 10^5 by a transimpedance amplifier. The amplified voltage (0-14V) was sampled by a digital acquisition board (National Instruments) that was controlled through a LabView virtual instrument.

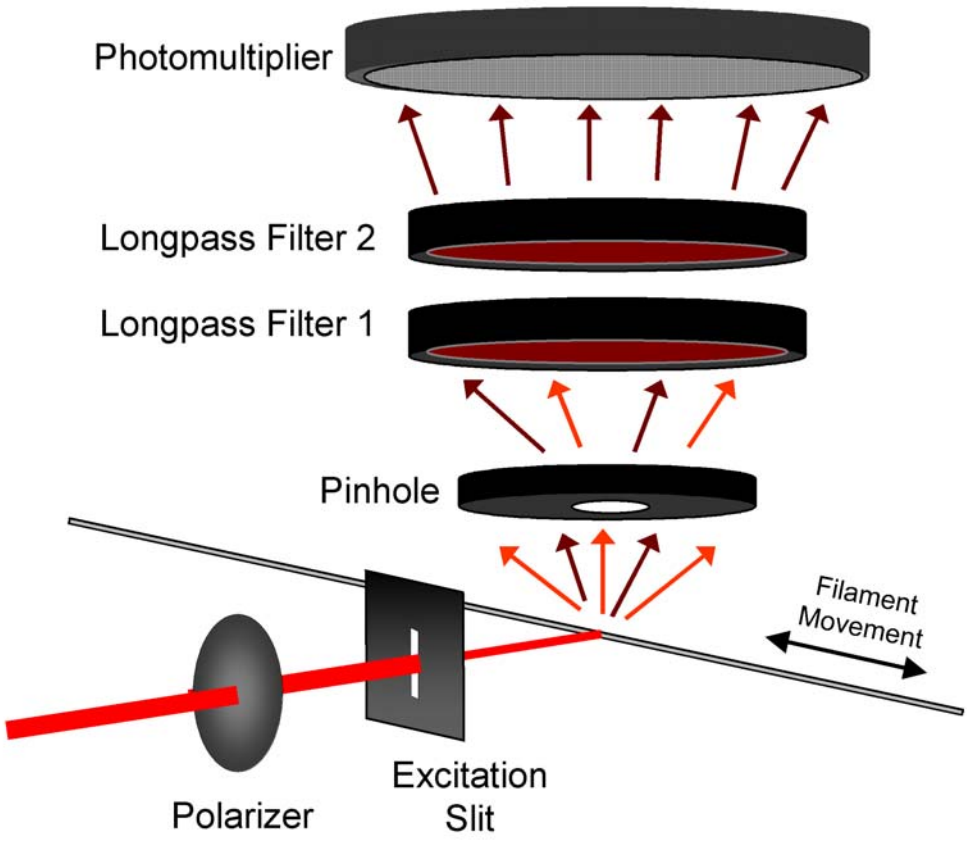

Figure 10. Optical path of virus detection system. Using a 638 nm laser excitation source, detection of filament fluorescence is possible using the appropriate emission filters. Exposure area on the filament is reduced by an excitation slit.

Filament movement and signal sampling were synchronized using a single LabView interface. Positive virus detection is defined as $p < 0.05$ for an unpaired t-test of capture antibody regions compared to control regions.

Experimental Parameters

Filament movement parameters were consistent throughout all experiments. Filament regions were oscillated back and forth 2 cm at 1 cm/s within each chamber for the requisite length of time, and filament speed in between chambers was constant at 2 cm/s. All filaments were blocked in Chamber 1 for 15 minutes before experiments were started. All experiments used M13K07 virus ($3.3x10^{10}$ virions/ml, unless otherwise noted) and used AF647 anti-M13 (20 μg/ml) for detection. Virus detection experiments differed only by incubation and wash times. SNR was defined as the average peak height of anti-M13 regions divided by average peak height of a negative control anti-E region. A standard unpaired t-test was used to compare average peak values with average anti-E values to determine statistical significance. P values less than 0.05 signified positive virus detection.

Basic system tests were performed to show the effectiveness of our optical system and to determine some standard parameters that help optimize signal to noise (Table 4). These tests were designed to show that FARA was capable of a high SNR and to show that laser exposure did not significantly bleach our labeled detecting antibody. Qualitative observations using our laser at full power (25 mW) previously showed that bleaching effects may be greater when the filament is still wet. To show that this effect was minimized with a less powerful laser beam, multiple laser scans of the same filament

were performed after a typical virus detection experiment. The filament was first scanned five times while wet. This same filament was allowed to dry and scanned an additional five times on the following day. The change in SNR with each scan was then calculated. Incubation parameters for these system tests are summarized in Table 4.

Once basic parameters were established, incubation times were shortened to determine the shortest assay time that resulted in positive virus detection. Virus and detecting antibody incubation times were shortened to one minute, and wash times were shortened to fifteen seconds. When this shortened assay time was established, experiments were performed to determine the limit of sensitivity of this technique and the minimum assay times required to detect lower virus concentrations. Virus concentration was reduced to 3.3×10^9 and 3.3×10^8 for these experiments, and virus incubation time was increased until detection was achieved. A summary of these parameters can be also be found in Table 4.

An important aspect of this optical system is the online detection and control of filament positioning. This permits decision on subsequent filament motion for additional incubation based on signal strength. This aspect could be very important for a new antibody/antigen pair for which optimal incubation times are not yet known or for rapid detection applications in which time is critical. In this approach a rapid detection protocol might be followed to detect a high virus titer and then a negative initial rapid screen might be followed up with a high sensitivity but slower detection protocol. A single filament was used to show that online detection could be utilized to increase signal strength. In the first experimental design, the filament was repositioned within the detecting antibody chamber to increase signal and then scanned again. In the second

experimental test the filament was repositioned within the virus chamber. In this test the first cycle of the experiment used a one minute virus incubation that yielded only a weak signal. Following this initial virus detection measurement, the capture antibody region of the filament was sent back to the virus chamber for additional incubation. After the additional virus incubation, processing within chambers 3-5 was repeated. The filament was cycled through this process three times to show the capability of using online detection and filament motion to enhance the fluorescence signal. Table 4 summarizes incubation parameters for both repositioning experiments.

Table 4: Incubation parameters for all experiments.

Experiment	Virus Time (min)	Wash (min)	Detecting Ab Incubation (min)	Final Wash (min)
Basic Detection	30	3	10	5
Bleaching Effects	30	3	5	5
Fast Detection	1	0.25	1	0.25
Virus Sensitivity	1,10,40	1	5	1
Detecting Ab Recycling	30	3	0.5, 1, 2	5
Virus Recycling	1,5,10	1	5	1

Results

As described below, recycling the regions of the filament containing the capture antibodies through the reaction chambers and re-positioning within the detector in an effort to increase signal was an important aspect of many experiments. One concern with this approach is the bleaching effect of laser illumination on the fluorescence compounds and on the antigen-antibody interactions. Therefore, we first verified that consecutive measurements of signal intensity produced similar intensities. Effects of laser illumination were investigated by taking multiple scans of two filaments following two virus detection experiments. Each filament was prepared with three anti-M13 regions and processed as summarized in Table 4. Previous observations had shown that bleaching may be more problematic for a filament if it remained wet while scanning. Therefore, one filament was kept wet during the five scans by cycling the filament back to the final wash chamber in between scans and another was allowed to dry before any scans were performed. As Figure 11 illustrates, full power laser illumination did appear to consistently decrease the observed signal. After five successive scans the signal was reduced to ~8% of its initial value (left bars of the left panel). If the filament was allowed to dry before measurements were made, the effects were negligible (left bars of the right panel). Allowing the filament to dry would add to the total processing time. Since rapid processing was one of the project goals, we first attempted to reduce the laser power and determine if this prevented the drop in signal intensity with subsequent scans. A polarizer was used to weaken the laser from its full strength of 25 mW to approximately 5 mW

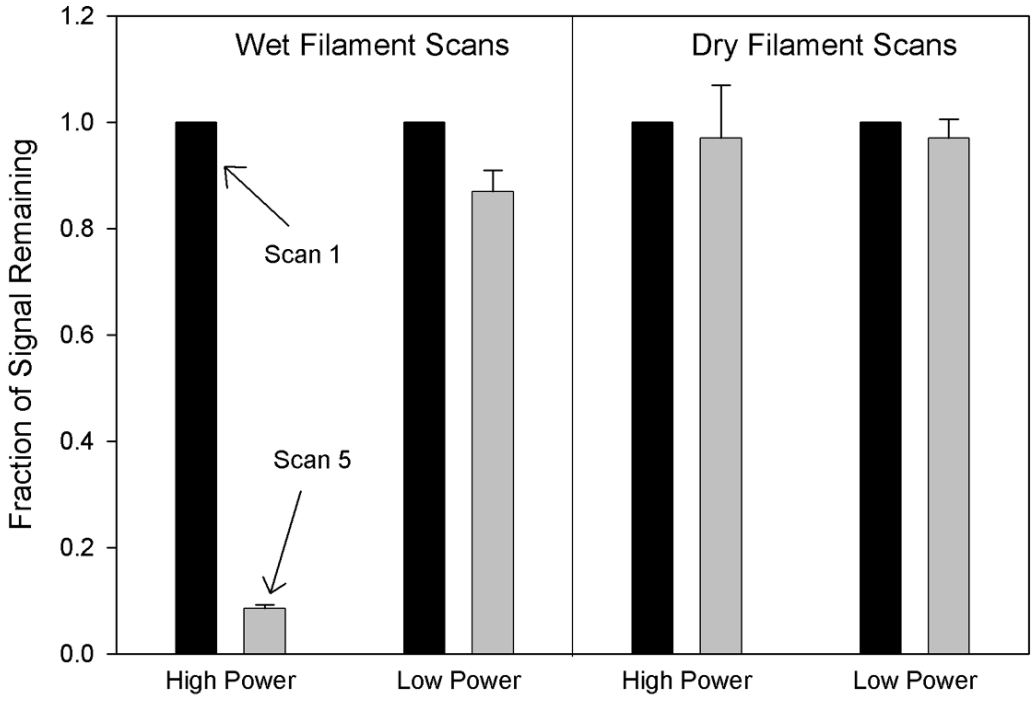

Figure 11: Repeated laser scans of virus detection filaments results in a significant signal drop for wet filaments using full laser power but not with low laser power (left panel). Repeated scans of dry filaments did not show significant signal loss for high or low laser power (right panel).

In addition, the filament scanning speed was increased to 4 cm/sec and an excitation slit was placed in front of the laser to further reduce laser exposure of the filament. As shown by the right hand bars in the panels of Figure 11, a reduced laser power did not change the signal intensity after five successive scans. All subsequent results were obtained with these laser power settings.

Figure 12 shows that regions of the filament containing the capture antibody anti-M13 produced strong fluorescence signals. In these experiments each ~3 cm length of the filament included one negative control anti-E region and three anti-M13 regions. After processing through the five chambers, strong fluorescence signal (SNR 51 ± 4.5) was observed in regions of the filament containing immobilized anti-M13 capture antibody, indicating successful virus detection The fluorescence observed in the region containing immobilized anti-E capture antibody has fluorescence that is indistinguishable from background. The lack of fluorescence in the anti-E region of the filament indicates that, as expected, antigen/antibody binding is a highly specific process and that no virus was attached to this region. In this system, higher virus concentrations could be detected with shorter virus incubation times. Figure 13 shows the virus incubation time required to detect virus of different concentrations along with the SNR achieved in each experiment. Detection of 3.3×10^8 virions/ml was achieved in 40 minutes and maintained a SNR of over 3. Raising the virus concentration to 3.3×10^9 virions/ml reduced the required virus incubation time to 10 min, while raising the SNR to over 6. A concentrations of 3.3×10^{10} virions/mL, the highest concentration tested, reduced the required time even further to only 1 minute and maintained a high SNR of almost 10.

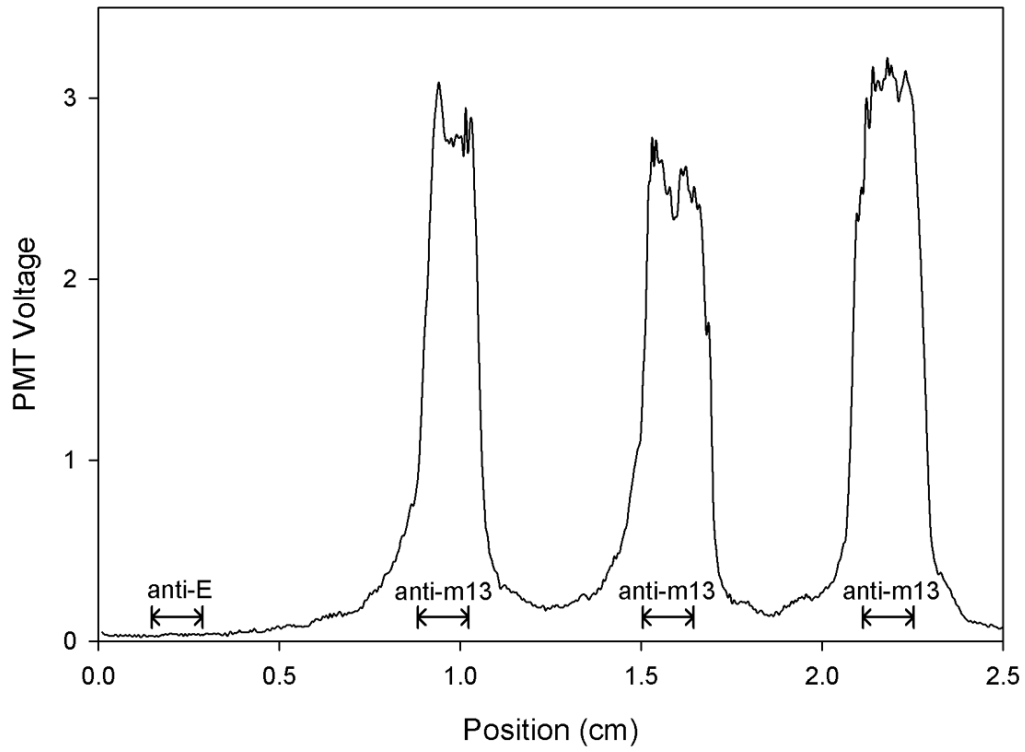

Figure 12: Photomultiplier output as a function of filament position. Laser scanning of the filament detects virus in all three antibody regions (anti-M13) with a SNR of approximately 51 ± 4.5. Control region (anti-E) is not distinguishable from background.

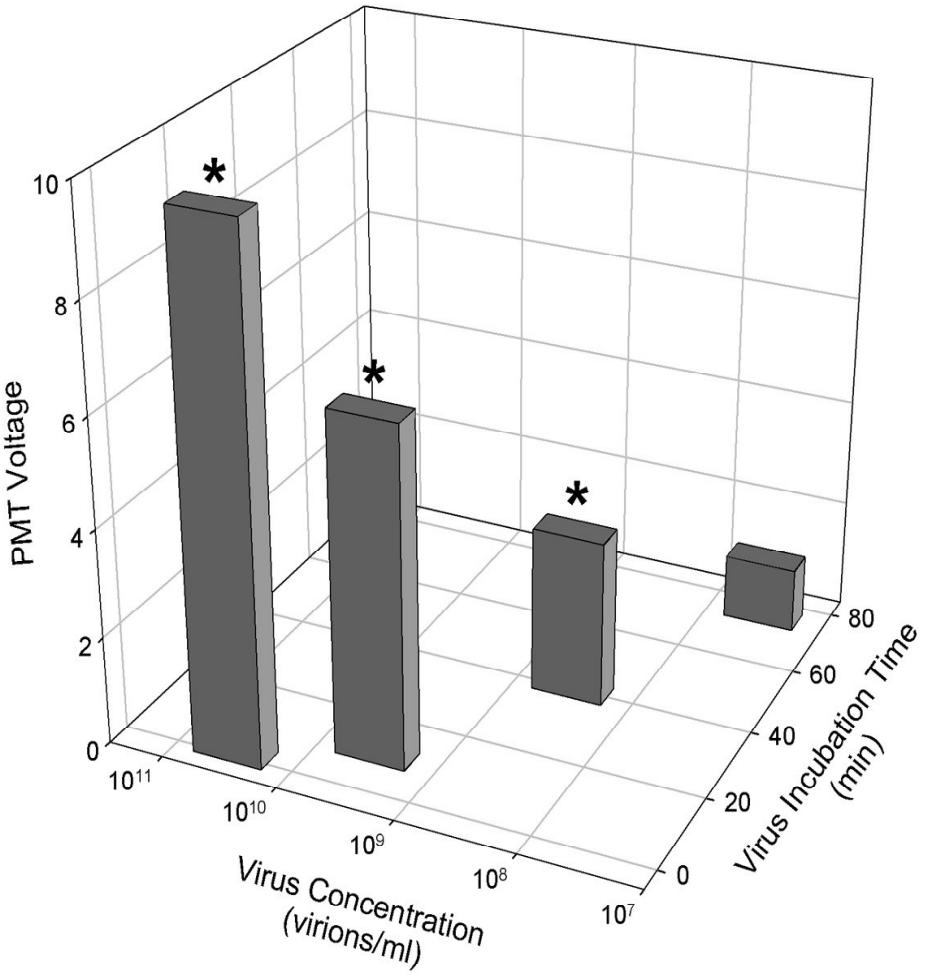

Figure 13: Virus incubation times required to detect different virus concentrations. A one minute virus incubation detected 3.3 x 10^{10} virions/mL with a SNR of nearly 10. Concentrations below 3.3 x 10^{8} virions/ml were not detectable with a 75 minute virus incubation time.

All other reaction parameters remained constant for these experiments (Table 4), so the total assay times for these trials ranged from 41.5 minutes for the lowest concentration to only 2.5 minutes for the highest concentration. Since filament blocking can be performed ahead of time, blocking times were not included in these estimates.

Online detection and control of filament position are unique aspects of FARA. In this approach, a weak signal could potentially be amplified by reprocessing the immobilized capture antibody regions through the reaction chambers. As an initial test of this strategy, experiments were performed to test the effects of re-positioning the capture antibody region of the filament within the detecting antibody chamber on detecting antibody interactions. The top panel of Figure 14 shows the increase in signal after the filament was cycled through the detecting antibody chamber three times for additional incubation. In this assay, signal strength increases by almost a factor of four as the filament is re-incubated.

Next, a second test of this strategy was performed by repositioning the capture regions within the virus chamber for increasing incubation times. In these experiments, a short initial virus incubation time was used for virus detection, so that fluorescence intensity was initially low. After the initial processing was performed and the filament scanned, the filament was repositioned within the virus chamber for an additional incubation, followed by the standard processing steps in the subsequent chambers. The bottom of Figure 14 shows the increases in signal for cumulative incubation times of 1, 5 and 10 minutes.

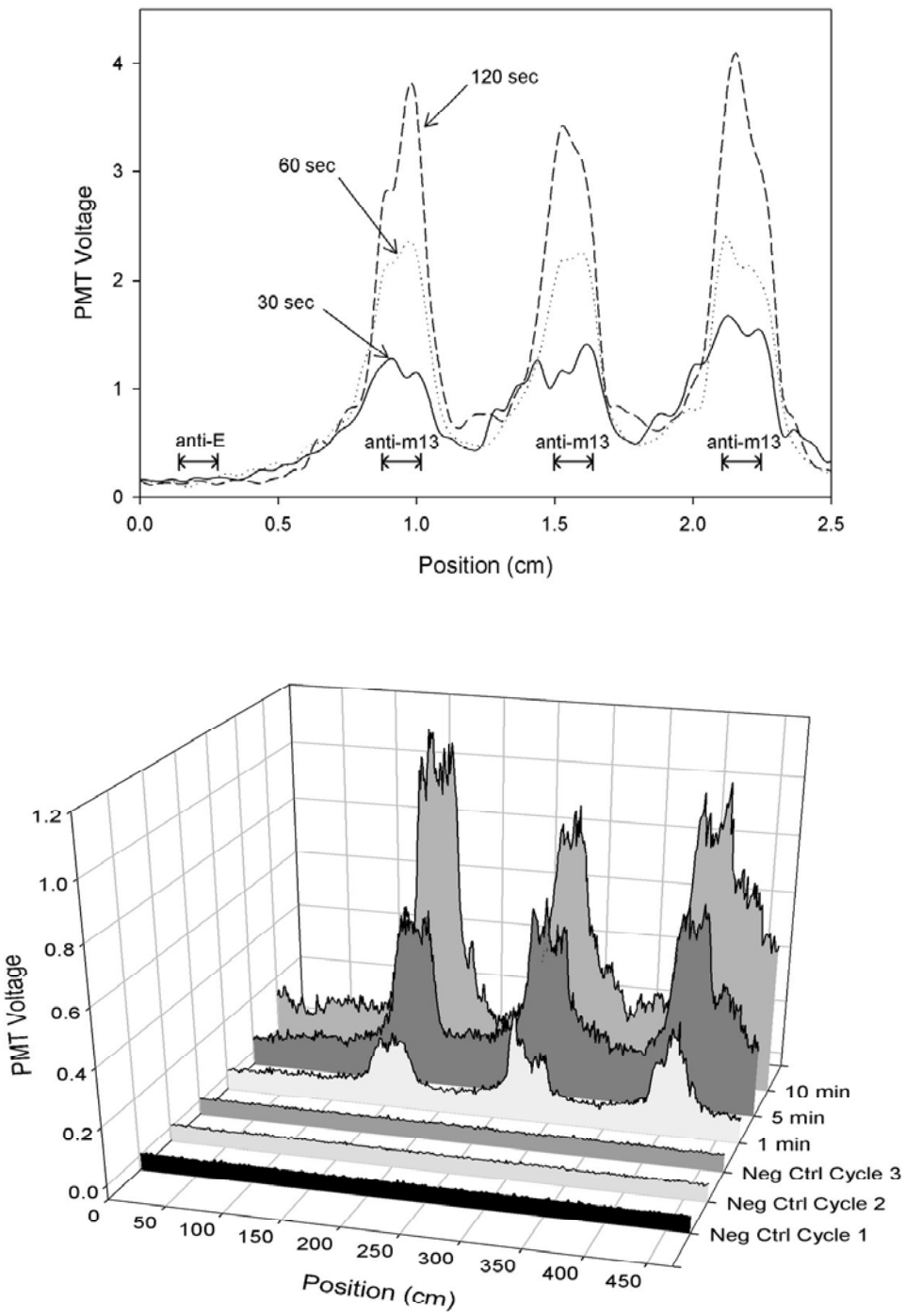

Figure 14: Signal increases as the capture region of the filament is cycled back to the detecting antibody chamber (top) or the virus chamber (bottom) for additional incubation.

The filament used for this experiment contained an anti-E negative control region on the left of the filament followed by three anti-M13 regions. Fluorescence increases approximately 4-5 fold for the anti-M13 regions from cycle 1 to cycle 3, but there is almost no change in the control antibody region.

As a final test of the filament repositioning strategy, we compared the signal intensities obtained with a single pass through the reaction chambers to the intensities obtained with filaments cycled through three successive processing cycles. As Figure 15 indicates, the reincubation strategy produced final signal intensities very similar to intensities of filaments with continuous incubation times when virus incubation times were matched. This indicates that filament motion and the processing steps does not reduce the observed signal. Furthermore, it suggests that using this system, flexible adaptive processing strategies utilizing repositioning of the filament after fluorescence measurements can be developed.

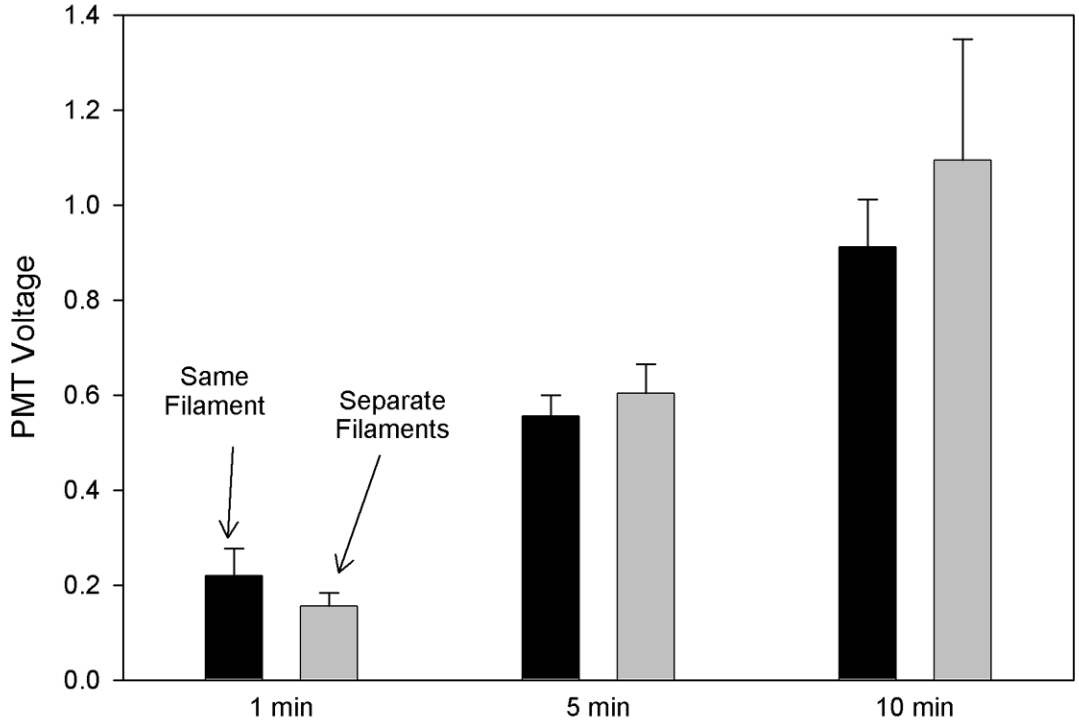

Figure 15. Comparison of recycling versus continuous virion exposure. Filaments repositioned within the virus incubation chamber (black bars) have fluorescence signals similar to filament incubated for the same time in one pass.

Discussion

Previous work on FARA has shown the potential of filament based virus detection (43). High levels of sensitivity and specificity have been shown, along with automated processing. However, automation was limited to filament processing, requiring filaments to be removed for fluorescence scanning on a microarray scanner. The focus of the present work is the design and development of a fluorescence-based online detector that is integrated with the existing system of microreaction chambers (Figure 9). Online fluorescence detection allows automation of the entire virus detection process with no user intervention. Figure 12 shows typical virus detection results using FARA's integrated optical detection system. The distinct peaks in the anti-M13 regions signify that M13 virus bound to these regions, which subsequently bound a fluorescently labeled detecting antibody, which is detected by an integrated detector. Specificity of virus detection is demonstrated by the lack of any detectable peak in the negative control anti-E region. Average SNR for this experiment was over 50, which exceeded any values previously reported for FARA, and assay time was shortened by at least 50% of previous values.

Much of the increase in SNR and decrease in assay time can be attributed to the optical flexibility of FARA's integrated detector. This detector allows any single filter or combination of filters to be used in the emission path. The ability to customize and adjust the emission filters is a major factor in the high SNR. Previously, detection was achieved using a dual laser microarray scanner with set emission filters that were not optimal for this application. Emission bandpass filters for the microarray scanner had a very broad bandwidth, so numerous fluorescent dyes could be used. However, these

broad emission filters also passed a significant degree of autofluorescence, which limited SNR. Future designs of FARA's integrated detector may eliminate most of the specular reflectance by mounting the PMTs at a 45° angle from vertical so that the line of reflection is not captured.

Laser power requirements for filament-based virus detection using FARA were not known, so a 25 mW diode laser was a cost efficient way to ensure that ample power was available. It was clear that bleaching of the detecting antibody could be a major issue if a filament was to be scanned multiple times. However, repeated, full power scans of a dry filament with multiple regions of immobilized positive control antibodies (AF647 anti-M13) showed little or no bleaching effects (data not shown). However, when filaments remained wet and underwent repeated scans, it became obvious that the laser at full power was having a detrimental effect on either detecting antibody fluorescence or on antigen-antibody interactions. A simple experiment that exposed the filament region of interest to laser radiation immediately after the virus incubation made it clear that the laser power was great enough to interrupt the bond between the antibody and virus.

The detection of fluorescence online and the filament movement control give FARA the unique advantage of rapid initial virus detection with subsequent high sensitivity for virus at low concentrations. Figure 14 shows how this feature can be used to optimize and increase signal. Fluorescence from the capture regions increases significantly after each additional incubation in both the virus chamber and the detecting antibody chamber. A region of interest on the filament can be processed and reprocessed until the fluorescence signal reaches a predetermined level. The virus detection program will continue to cycle the filament back through the reaction chambers until the signal

reaches this level or until total assay time has reached a preset time. This could be very useful for a different antigen/antibody pair when optimal incubation times are not known. On-line fluorescence detection could also be very valuable tool for guiding further testing. Multiple groups of antibody regions, each corresponding to a different test, could be immobilized along a long filament. The results from one group could determine which group is tested next. In this manner, a sample could be probed for many antigens in the order which best preserves sample and provides the maximum information about the unknown sample.

Our initial laser detection system appeared to decrease the observable signal intensities seen in subsequent readings. Initial experiments utilized the excitation laser at its full strength of 25 mW, but qualitative observations indicated that repeated laser exposure at this intensity reduced fluorescence not only through bleaching effects, but also possibly through an unidentified interruption of the antibody-antigen interaction. Experiments exposing the filament to the laser as it exited either the virus chamber or the final wash chamber helped distinguish between bleaching effects and the effects on antibody-antigen interactions. In both experimental designs, repeated scans reduced the signal intensity. Exposure of the filament to the laser immediately after the virus chamber reduced the SNR by a factor of four, indicating the antibody-antigen interactions were being disrupted since no labeled antibody was present at the point in the assay. When the filament was exposed to the laser following the final wash, SNR was also reduced by approximately a factor of four, indicating that bleaching of the fluorophore is occurring. Based on these observations, we conclude that laser interactions with both the fluorophore and the antibody-antigen binding partners contributed to the decline in signal

intensity. Beaching effects are well known, however there appear to be few reports or studies directed at the effects of antibody-antigen binding.

Since laser power appeared to be important, we also estimated the light exposure produced under the conditions of these experiments. The calculated laser exposure for each capture region of the filament using full laser power was approximately 1.13 mJ during scanning. This calculation was based on the laser power (25 mW), region width (1.5 mm), scan speed (0.5 cm/s), and the width of the filament relative to the laser beam. The antigen-antibody interaction is typically made of several non-covalent interactions such as hydrogen bonding, dipole-dipole interactions, hydrophobic interactions, Van der Waals forces, and sometimes electrostatic interactions. The strength of the overall interaction is a summation of these individual interactions with electrostatic interactions and hydrogen bonding being the strongest bonds at 670 kJ/mol and 20 kJ/mol, respectively. The strength of the antibody-antigen bond is strongly dependent on the proximity of the contact areas between the antibody paratope and the binding epitope on the antigen. Since every interaction is different, the total energy of such interactions may range from the 10's to 100's of kJ/mol. Even if it is assumed that 100% of the antibody from the spotting solution adsorbs to the filament and binds virus after the initial washing and blocking step, there is still ample laser energy to disrupt all virus-antibody interactions if all laser energy were completely absorbed by the surface molecules. However, an accurate calculation of this energy is not possible due to two major unknowns. It is unknown how much antibody from the initial spotting solution binds to the filament and how much remains active. In addition, the energy transferred from the laser beam to surface antibodies on the filament is also difficult to calculate. Even

though the laser exposure is easy to estimate, the amount of adsorbed laser light is still unknown. Most of the absorption of laser light is by the filament itself, so it remains unclear how much of this energy is being transferred to the antibodies and antigens on the filament. Since the laser is at a wavelength (638 nm) that is not highly absorbed by proteins, the antibodies themselves should not absorb a significant amount of energy. Nevertheless, laser exposure at full power was shown to be harmful to virus binding. Weakened interactions between virus and antibody allowed the virus to be washed off when the capture regions were sent back through the system for additional incubations. To limit these effects, a polarizer was placed in front of the laser and adjusted so that the laser output was reduced to 5 mW. To reduce exposure even further, the filament scanning speed was increased to 4 cm/sec and an exposure slit was built to reduce the area of the filament that was illuminated by fifty percent. These modifications reduced filament exposure by a factor of 100 to approximately 0.014 mJ, and laser effects were minimized.

Conclusion

In summary, the addition of an online optical fluorescence detector increases the sensitivity of FARA and provides additional processing flexibility that makes adaptive detection feasible.

CHAPTER V

AUTONOMOUS REOVIRUS STRAIN CLASSIFICATION USING FILAMENT-COUPLED ANTIBODIES

Gregory P. Stone[1]
J. Denise Wetzel[2,4]
Terence S. Dermody[2,3,4]
Frederick R. Haselton[1]

[1]Department of Biomedical Engineering
Vanderbilt University
Nashville, TN

[2]Departments of Pediatrics and
[3]Microbiology and Immunology
[4]Elizabeth B. Lamb Center for Pediatric Research
Vanderbilt University School of Medicine
Nashville, TN

(This manuscript will be submitted for review to *Journal of Immunological Methods)*

Abstract

We have previously described the development of a filament-antibody recognition assay (FARA) that creates ELISA-like sandwich structures by positioning a monofilament containing regions of immobilized antibodies through a series of reaction chambers. One of these chambers contains the unknown virus solution and when the appropriate filament-coupled antibody is present in this chamber, virus is coupled to the filament. Virus detection is achieved by subsequent positioning of the filament within a solution of fluorescently labeled detection antibody, and passing the filament through an integrated fluorescence detector. In this report, we describe the application of this technology to subtype reovirus. We have developed a decision tree that tests for virus with increasing specificity at each level of the tree. Using three types of reovirus and one bacteriophage, our system correctly detected and identified all three reoviruses at a concentration of 2×10^{12} virions/ml and M13K07 phage at 3×10^{11} virions/ml. Fluorescence from all peak regions was determined to be significantly higher than background regions ($p < 0.005$). T3D reovirus diagnosis required three levels of testing and resulted in signal to noise ratios (SNR) of 11.5 for general reovirus testing in level 1, 9.8 for serotype 3 identification in level 2, and 3.3 for final T3D identification in level three. T3SA+ also required three levels of testing before a final diagnosis was returned in level 3. A SNR of 8.8 for general testing, 8.3 for serotype 3 identification, and an expectedly low 1.1 for level three testing was found. T1L was identified in two steps with a SNR of 6.4 and 5.1. M13K07 phage detection only required one step for identification and resulted in a very high SNR of 88. Reovirus provided a simple test system to prove the feasibility of a decision scheme that uses online feedback to guide

additional testing, but this scheme could easily be expanded into a much more complicated system with numerous levels and branches.

Introduction

Although the advancement of modern medicine has led to the eradication of many diseases in this country, diagnosis and treatment for the common cold have lagged far behind. The economic impact of this illness to this country is estimated to be in the tens of billions of dollars through missed work and low productivity on the job. When caregiver absenteeism is included, this figure jumps into the hundreds of millions of dollars (50,51). Although the development of new antibiotics and anti-viral drugs has made significant progress, treatment and diagnosis of the common cold is often complicated by the inability to accurately diagnose the etiology behind the illness in a clinical setting (52,53).

In a research laboratory setting, a specific cause of infection can usually be found by utilizing a variety of diagnostic tests. In a majority of patients displaying symptoms associated with the common cold, a viral etiology has been shown, with the rhinovirus being responsible for 30-50 % of infections. Coronaviruses, influenza virus, respiratory syncytial virus, parainfluenza, adenoviruses, and enteroviruses cause a vast majority of the remaining viral infections (51,53-57). Different pathogens often require different techniques for optimal detection, so there is no single method that provides accurate diagnosis of every likely pathogen. Compounding this problem is the fact that each of these major pathogens may have numerous subtypes. Rhinoviruses and influenza each have over one hundred different variants, making traditional serological techniques difficult and often unreliable (58,59). However, in a clinical setting, it is often not feasible to spend the time and resources to identify a distinct causative agent. Although most studies of the common cold have shown a bacterial etiology in only a small percent

of cases, the lack of a definitive viral diagnosis in a clinical setting continues to lead many physicians to prescribe antibiotics as treatment for the illness (3,51,60,61). This misuse of antibiotics has led to an increasing number of antibiotic-resistant bacterial infections.

A quick, reliable technique for detecting such a wide range of pathogens does not exist. In the research lab, traditional techniques such as virus isolation, microscopy, and serology are used, along with more modern strategies such as direct antigen detection (ELISA) and PCR to determine the infectious agent. A simpler strategy that could combine the reliability of traditional techniques with the sensitivity and quickness of modern techniques would be very advantageous in a clinical setting. We have designed a system that could eliminate the need for such a wide panel of tests. (43,62). We have a designed a filament based detection strategy where specific antibodies are passively immobilized in a linear array along the surface of a monofilament. The filament is pulled through a series of small reaction chambers where the antibodies pull the corresponding virus out of solution, if present. A fluorescently labeled second antibody is then used to detect bound virus using a laser excitation source and photomultiplier tube. The results of each test are then fed back to a computer control program, so that the computer can decide if further testing is necessary. Using this scheme, the first set of immobilized antibodies corresponds to general virus classes. If a virus is found, the program moves the filament so that the next set of antibodies tested corresponds to one of many subtypes of the virus found in test one. In this manner, each subsequent test becomes more specific for a single antigen, and subtypes of viruses not found in the early tests are

ignored. This strategy limits the overall amount of testing as major virus classes are ruled out in the early stages.

We have developed an automated system that uses pre-programmed parameters in a knowledge-based decision tree that is increasingly specific in each level (Figure 18). We show the effectiveness of our automated system and our decision tree strategy to detect the presence of reovirus in solution. Using a set of reovirus subtypes and one bacteriophage, we use a three level decision tree to determine the reovirus subtype. As a human pathogen, reovirus is an excellent test system to show the clinical implications of our system, while safety concerns were minimal since reovirus infection in adults is very rare.

Methods

FARA: Filament Antibody Recognition Assay

A polyester filament (120 μm OD, Sulky Invisible, Punta Gorda, FL) with circumferential bands of immobilized antibody was passed through a series of five glass micro-reaction chambers that are similar to the five major steps of an ELISA. Table 5 gives an overview of the purpose and contents of each chamber. Antibody regions were first rehydrated, and the bare regions of filament were blocked from non-specific binding of virus. Following this step, the immobilized antibody region was incubated in the virus chamber for 40 min where virus was captured out of solution if the corresponding antibody was present on the filament. Following virus incubation, unbound virus was briefly washed away in step 3, before exposure to a fluorescently labeled second antibody in step 4. .The labeled antibody solution in step 4 contained fluorescently labeled

antibodies specific to each test virus. Bound virus from step 2 captured its corresponding fluorescent antibodies. A final wash in the last step removed any unbound reagents, and the region of interest was pulled through an integrated fluorescence detector.

Hardware

Chambers and Stage. Glass micro-reaction chambers were cut from 1/4-inch stock tubing into 75 mm lengths, and the ends were flared outward to facilitate movement of the filament through the chambers. Interior diameters of the chambers were 2 mm or 0.75 mm (See Table 5) Chambers were arranged linearly on the top of a horizontal aluminum stage using machined aluminum mounts. Linear position of the chambers could be finely adjusted due to the oblong mounting holes on each mount.

Filament Control. Movement of antibody bands through the chambers was done with a rotary stage and control unit from Yaskawa Instruments (Waukegan, IL) and controlled by a LabView Virtual Instrument (VI) interface (National Instruments, Austin, TX). The motor wound and unwound the filament around a spindle to move the region of interest forward and backwards. A small weight was placed on the opposite end to keep a constant tension on the filament.

Table 5: Purpose and contents of glass reaction chambers. *PBS with 0.1 % Tween 20 as a blocking agent

Step	Description	Solution	Incubation Time	Chamber ID
1	Block/Wash Filament	PBS-T*	15 min	2 mm
2	Virus Incubation	Unknown Virus Solution	40 min	0.75 mm
3	Wash	PBS-T	1 min	2 mm
4	2^{nd} Ab Incubation	Flourescently labeled 2^{nd} Antibody	5 min	0.75 mm
5	Wash	PBS-T	1 min	2 mm

If extremely long filaments were required, the distal end could be looped back around to the spindle using a small pulley so that excess filament could be wound back around the spindle as the antibody regions move through the system. However, following fluorescent scanning for most experiments, filament regions were cut and scanned again in a GenePix 4000B microarray scanner (Axon Instruments, Union City, CA). Parameters such as filament speed and residence times within chambers were all controlled through the LabView VI.

Lasers and PMTs. The online fluorescence detector was comprised of a central sample chamber through which the filament was passed during detection. Laser excitation sources were attached to either side of the chamber as shown Figure 16. Laser 1 was a 25 mW, 638 nm diode laser (Coherent, Santa Clara, CA) and was used to excite Alexa Fluor 647 fluorescent dye (AF647, Molecular Probes, Eugene, OR). Laser 2 was a 532 nm, 20 mW diode-pumped, solid state laser (B&W Tek, Inc., Newark, DE) and was used to excite Alexa Fluor 555 dye (AF555, Molecular Probes, Eugene, OR). Laser one was attenuated with a polarizer and an excitation slit, reducing the effective laser power to approximately 5 mW. Laser 2 was not attenuated. Two Hamamatsu R928 photomultipliers were attached to the top and bottom of the sample chamber and were powered by 850 V and 800 V signals for AF647 and AF555 channels, respectively. Current from the PMT was converted to a voltage using transimpedance amplifiers that amplified the signal by a factor of 10^6 for AF647 and 10^5 for AF555. Voltage was sampled at a rate of 800 samples/sec using a digital acquisition board from National Instruments, and signal acquisition was synchronized with filament movement using LabView.

Filters. Long pass filters with cutoffs at 685 nm (Chroma, Rockingham, VT) and 665 nm (Melles Griot, Rochester, NY) were combined to filter out reflected laser light from the AF647 channel. For the AF555 channel, two long pass filters (570 nm cutoff, Melles Griot) were stacked with a bandpass filter centered at 565 nm (30 nm bandwidth, Chroma) to filter out reflected light. Filter sets were placed in the light path between the sample chamber and the PMTs.

Feedback Control

Spatially localized fluorescence from the filament was measured as a 0-14 V signal from the transimpedance amplifier. Voltage data from the scan was passed back to a peak detection program in LabView that identified all peaks present in the data, the location of each peak, and the amplitude of each peak. Peak detection threshold parameters were user defined as 0.3 V (approximately three times background), with a width of 30 points. Although 30 pts represents a width slightly larger than the physical tooth width of the comb, antibody spots tended to be drawn out slightly from the edges of the tooth. A width of 30 points minimized the false positives using the peak detection program. Red fingernail polish was used as a visible and fluorescent marker to identify spotted regions during experiments and during laser scanning. The fluorescent fingernail polish marks resulted in sharp peaks in all situations. Since the physical location of the immobilized antibody regions in between the markers was known, experiment conclusions were based on the distance of the second detected peak from the initial fluorescent marker.

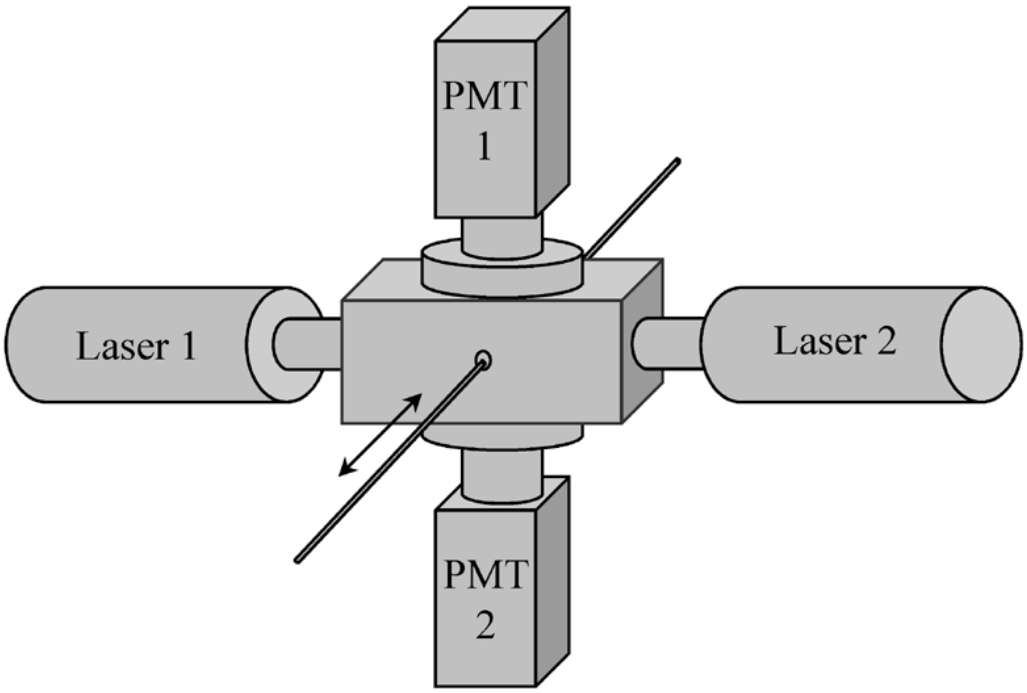

Figure 16: The filament passes through a rectangular sample chamber that has two laser excitation sources attached to either side. Photomultiplier tubes are attached to the top and bottom of the chamber.

If no peaks were found within the fluorescent markers, the program stopped and indicated to the user that no virus was found. Similarly, if a peak was detected in the negative control region of the filament, the program stopped and indicated contamination to the user. If peaks were detected within the region, the program moved the filament downstream to the appropriate antibody region for more specific testing. Downstream regions were identified by additional fluorescent markers on the filament. The VI moved the filament forward until the appropriate set of markers was detected, indicating that the appropriate antibody region was ready for incubation in chamber 1. This process was repeated at each level of testing. As an additional check, data obtained with each filament scan was loaded into a MATLAB program that allows the user to mark the locations of each antibody region. The program calculates the mean and standard deviation of each region selected, and a paired t-test was used to compare capture antibody regions with negative control regions. A p-value less than 0.05 signified positive virus detection.

Reagents

Cells and viruses. Murine L929 (L) cells were cultured in suspension in Joklik's modified Eagle's medium supplemented to contain 5% fetal bovine serum, 2 nM $_{L}$-glutamine, 100 U/mL penicillin, 100 μg/mL streptomycin, and 0.25 g/mL amphotericin-B. Reovirus strains T1L and T3D are laboratory stocks. T3SA+ and T3SA- are monoreassortant viruses isolated from L cells that were mixedly infected with T1L and either T3C44MA (for T3SA+) or T3C44 (for T3SA-). T3C44 is a reovirus field isolate strain that does not bind sialic acid. This virus previously was used to infect murine

erythroleukemia (MEL) cells, which require sialic acid binding for efficient reovirus infection. T3C44MA was isolated from T3C44-infected MEL cells after several passages and is capable of binding sialic acid (63). T3SA+ and T3SA- contain the S1 gene segment, which confers sialic acid binding capacity, from the respective type 3 parental strain and all other gene segments are from T1L. Reovirus purification was performed as previously described (63-65). Briefly, L cells were inoculated with second passage L-cell lysate stocks of twice plaque-purified reovirus at a multiplicity of infection of 10 viral particles per cell. Virus was purified from infected cells by freon extraction and CsCl-gradient centrifugation. M13K07 purified virus was obtained from the Vanderbilt Molecular Recognition Core.

Antibodies. Mouse monoclonal reovirus antibodies 4F2, 5C6, and 9BG5 were purified from hybridoma supernatants using Protein A column chromatography. Reovirus antibody 8H6 was obtained from the Wilson laboratory (Department of Pediatric Infectious Disease, Vanderbilt University). Anti-M13 monoclonal antibody was purchased from Amersham Biosciences (Piscataway, NJ).

4F2 and 8H6 used in Step 4 for fluorescence detection were labeled with AF555 or AF647, respectively, according to the manufacturer's instructions. Labeled antibody was purified using PD-10 size exclusion chromatography columns (Amersham Biosciences). The concentration and degree of labeling for labeled antibodies was determined using absorbance measurements at 280 nm and at the peak absorbance wavelength of each dye. Aliquots of both labeled and unlabeled antibodies were stored long term at –20 °C, while working solutions were kept at 4 °C. Dilutions of antibodies were made immediately prior to experiments.

Preparation of Immobilized Antibody on Filament

Filament regions for immobilizing antibody were placed across the concave teeth of a PhastGel sample applicator (Amersham Biosciences) so that antibody spotting could be localized to a distinct region (Figure 17). Surface tension within the teeth of the comb kept the antibody from spreading along the filament, allowing for a small distinct spot. Antibody was spotted (0.75 μL), and was allowed to passively adsorb to the filament for 45 minutes in a humidified box. Following incubation, filaments were rinsed in PBS-T and threaded through the reaction chambers for virus detection experiments. Experiments were performed to determine the optimal concentration of each antibody. Anti-M13, 9BG5, and 5C6 were spotted at concentrations of 0.5, 0.25, and 0.2 mg/mL, respectively. When multiple sets of immobilized antibody was required, multiple sample applicators were fastened together and excess filament was wound in between regions to assure adequate spacing of the regions.

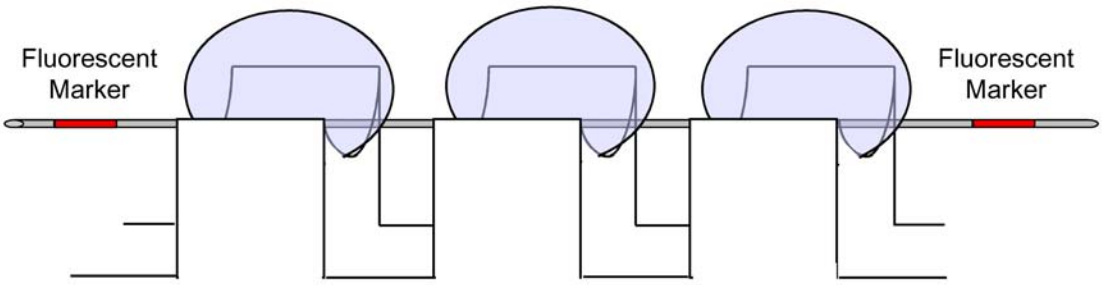

Figure 17: Filament is placed within the concave teeth of a PhastGel applicator to keep the spotted antibody localized to a small region.

Experimental Parameters

Virus detection parameters were constant in all experiments. Incubation times for each chamber are summarized in Table 5. While in each chamber, the region of interest was oscillated 2.5 cm at a speed of 1 cm/sec to increase interactions between immobilized antibody and virus particles in solution. PBS-T was used in all wash chambers and was used for virus and labeled antibody dilutions. Concentration of all reovirus virus solutions was 2 x 10^{12} virions/mL. AF647-8H6, AF555-4F2, and AF647-anti-M13 detecting antibodies were mixed at a concentration of approximately 40 μg/mL for each antibody. The organization of immobilized antibody bands within each region of interest depended on the level of testing. The region of interest for level one contained a PBS negative control spot, followed by a spot of mixed 9BG5 and 5C6 (0.25 mg/mL, 0.2 mg/mL), and an anti-M13 spot (0.5 mg/mL). Levels two and three included a negative control PBS spot followed by separate 9BG5 and 5C6 spots (0.25 mg/mL, 0.2 mg/mL). Solutions were pipetted into appropriate chambers and used for all three levels of testing. If testing proceeded all the way to level three, fluid loss from the chambers was monitored and replenished if necessary.

Results

The LabView VI coordinated all filament movement, filament scanning, and signal feedback into one program. As described above, this detection system was designed to automatically detect the presence of reovirus or M13K07 with increasing specificity as testing proceeded from start to finish. Below is a summary of antibody specificity for each test virus:

M13K07 → anti-M13
T1L → 5C6, 8H6
T3SA+ → 9BG5, 8H6
T3D → 9BG5, 8H6, 4F2

Our LabView program resulted in a theoretical decision tree as depicted in Figure 18. If fluorescence was detected from the anti-M13 region of the filament, the program returned a diagnosis of M13K07 virus, and no further testing was necessary. If fluorescence was detected in the 9BG5/5C6 region, the program returned a general diagnosis of reovirus and advanced the filament to the appropriate region for level 2 testing, where a more specific test for reovirus was performed. In level 2 testing, fluorescence from the 5C6 region indicated a serotype 1 reovirus, which, in this scheme corresponded to T1L reovirus. A diagnosis of T1L represented an endpoint in the decision scheme and testing stopped. Fluorescence from the 9BG5 region indicated the presence of a serotype 3 reovirus, and the program advanced the filament for further subtyping in level 3. Level 3 testing utilized AF555 4F2 antibody as the detecting antibody and used a second detection channel with a green excitation laser to differentiate between different serotype 3 reoviruses. If fluorescence was found in the 9BG5 region using this channel, a diagnosis of T3D reovirus was returned and testing along that branch ended. When no fluorescence was detected from the second channel for that region, the program ended with a diagnosis of T3SA+/T3SA- reovirus.

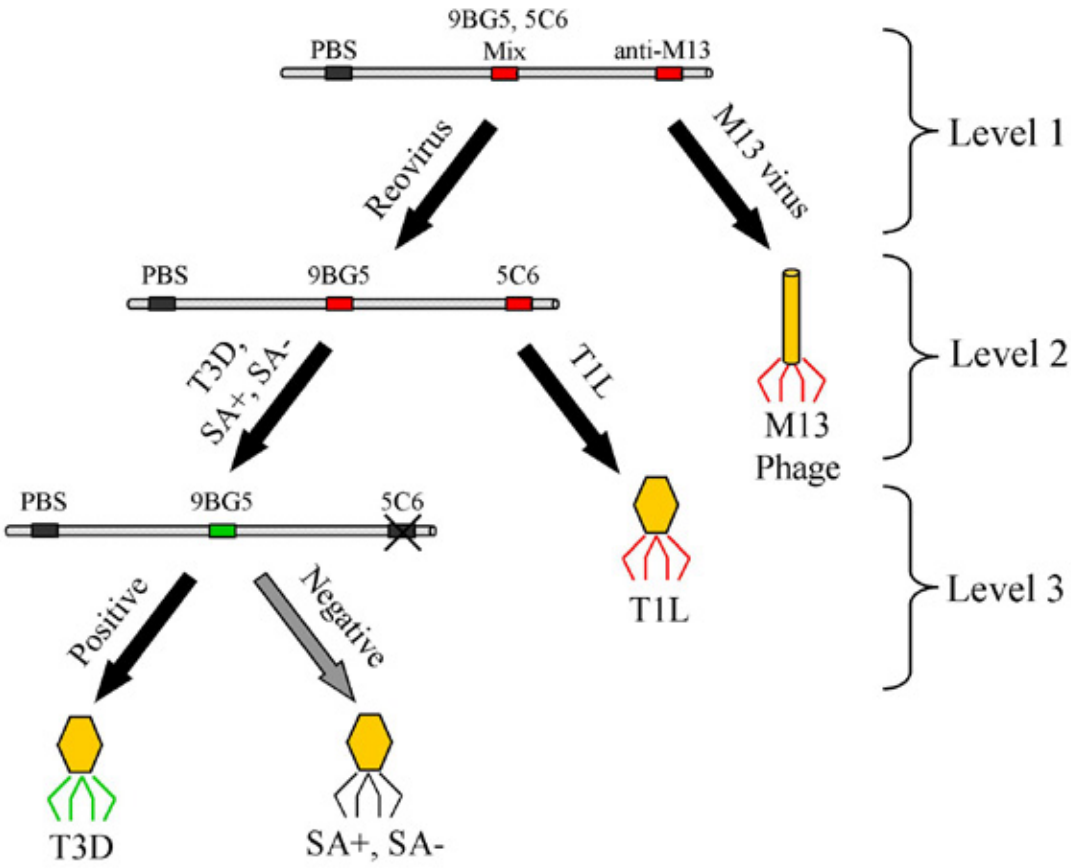

Figure 18: Testing was divided into three levels of specificity. The LabView control program began at level one and followed different branches of this decision tree based on the type of virus found at each level. When reovirus was detected in level one, filament was moved forward to the next antibody region for level 2 testing. If a serotype 3 reovirus was found (T3D, SA+, SA+) in level 2, testing continued for one more level to distinguish between these types. Negative control PBS spots were included in each testing region. Fluorescence detected in these negative control regions indicated contamination, and the program returned an error message.

Fluorescence detected in the negative control PBS regions of any level indicated contamination, and the program stopped and returned an error message to the user. This situation did not arise during testing.

Figure 19 illustrates the specificity of each test antibody towards its corresponding virus. Results shown correspond to each level of the decision tree that pertained to each of the four test viruses and show fluorescence (as voltage) as a function of filament position for separate filaments. After each experiment, filaments were also scanned in a microarray scanner, and the resulting images are included at the top of each panel. The top panel shows a distinct peak for each curve in the 9BG5 antibody region, indicating successful detection of T3D. The red curve corresponds to level 1 and level 2 testing that used AF647-8H6 as the detecting antibody, while the green curve corresponds to level 3 testing that used AF555-4F2 and the second detecting channel. Neither curve shows cross reactivity of T3D reovirus with the immobilized 5C6 region or negative control PBS region.

The second panel of Figure 19 shows the equivalent data set using the T3SA+ reovirus where the red curve corresponds to level 1 and level 2 testing, and the green curve corresponds to level three testing. As expected, fluorescence is detected from the 9BG5 region using AF647-8H6 detecting antibody (red curve) but not when using AF555-4F2 antibody and the second detecting channel as is done in level 3 testing (green curve). No detectable cross reactivity is found in the 5C6 antibody region or negative control region.

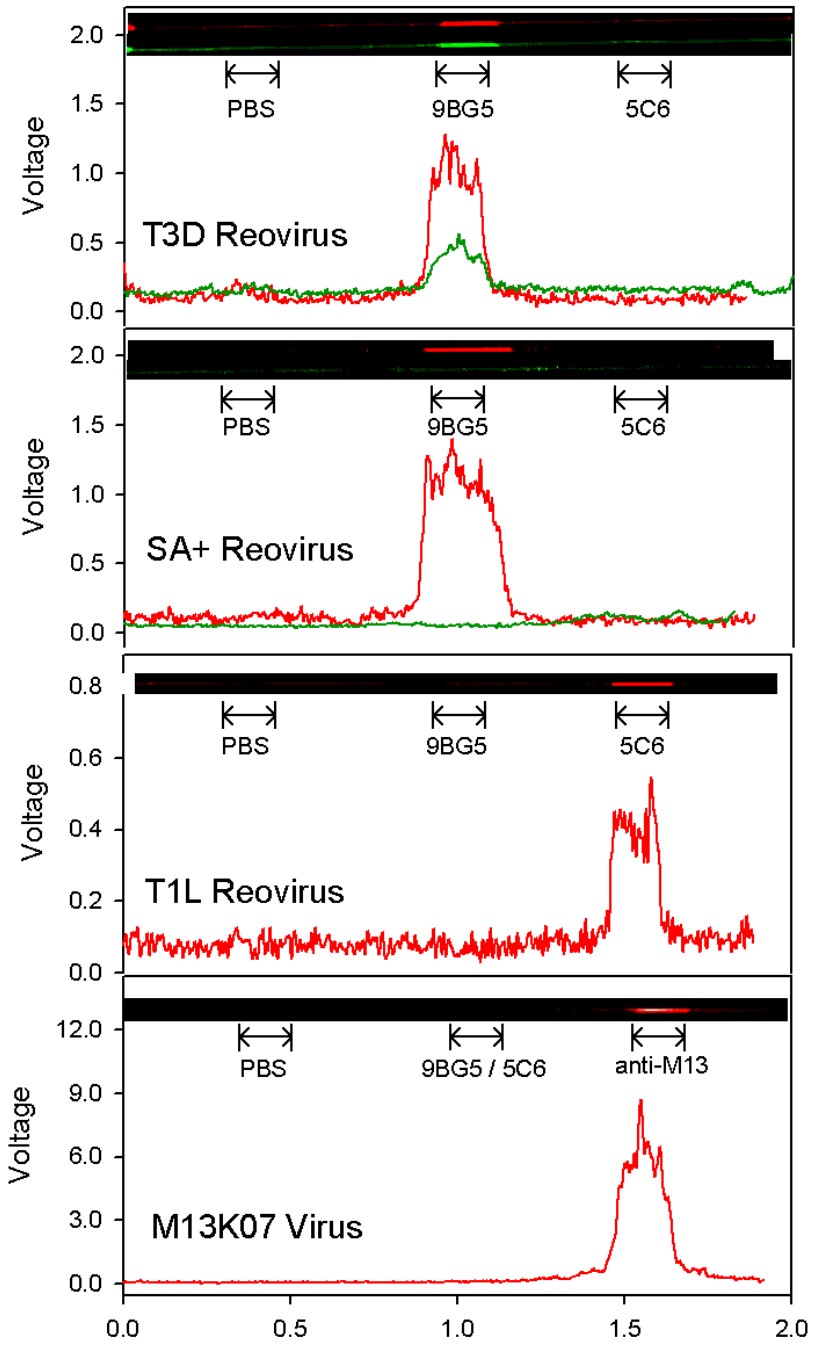

Figure 19: Immobilized antibody on the filament detects reovirus and M13K07 phage using AF647-8H6 (red) or AF555-4F2 (green). Top two panels also show specificity of AF555-4F2 for T3D over SA+ corresponding to level 3 testing. Line graphs represent data from online detection. Images were obtained using a dual laser flatbed microarray scanner.

Detection results for T1L virus are shown in the third panel of Figure 19. Only one curve is shown, corresponding to level 1 and level 2 testing since T1L testing does not continue in level 3. The expected fluorescence is detected in the 5C6 antibody region, and no distinguishable fluorescence is seen in the 9BG5 or PBS regions. The bottom panel of Figure 19 shows results using M13K07 analogous to level 1 testing. Strong fluorescence is seen in the anti-M13 region but not in the 9BG5/5C6 or PBS regions, which was expected. The four panels of Figure 19 represent each level of detection of the decision structure shown in Figure 18, and no detectable cross reactivity was seen at any of the three levels.

The LabView decision making process is based on the presence or absence of fluorescence peaks at known locations along the filament, so peak height is not taken into consideration when making the diagnosis. Table 6 shows results from multilevel, automated detection of each virus. The left side shows the layout of antibody regions for each level. The table on the right shows the location of peaks detected at each level of the automated experiments and the corresponding LabView diagnosis. For all multi-step experiments, LabView diagnosed the virus with greater specificity at each level. For each reovirus tested, level 1 resulted in a general identification of reovirus, so testing continued in level 2 where diagnosis became more specific and differentiated between serotype 1 (T1L) and serotype 3 (T3SA+, T3SA-, and T3D) reovirus. For T1L, testing stopped here after a positive result, but for serotype 3 viruses, testing continued one step further.

Table 6: Automated virus detection and diagnosis for each test virus. The figure on the left shows the layout of immobilized antibody regions for each level. The table on the right side shows the location of peaks found by LabView during automated, multilevel detection, along with the corresponding LabView diagnosis. For each virus, diagnosis gets more specific with each level of testing.

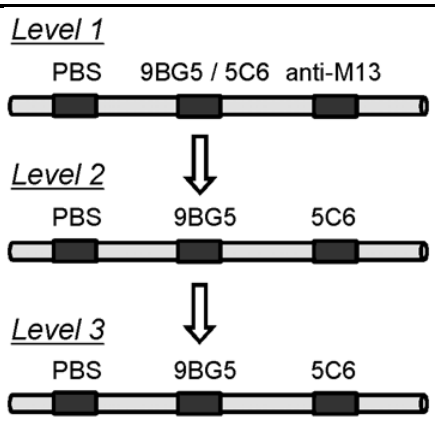

Virus	Level	Peak Position	LabView Diagnosis
T3D	1	9BG5/5C6	Reovirus
	2	9BG5	Type 3 Reovirus
	3	9BG5	T3D
T3SA+	1	9BG5/5C6	Reovirus
	2	9BG5	Type 3 Reovirus
	3	None	T3SA+
T1L	1	9BG5/5C6	Reovirus
	2	5C6	T1L Reovirus
M13K07	1	Anti-M13	M13K07

Step three diagnosis depended on the presence of a peak in the 9BG5 region for a positive T3D result and the absence of a peak for a SA+ or SA- positive result. M13K07 diagnosis was made in one step, so no further testing was necessary.

Since LabView Diagnosis was based only on the presence or absence of fluorescence peaks, an independent statistical analysis was made using MATLAB to make sure each peak found was statistically significant when compared to background values. The MATLAB program calculated the average and standard deviation of each antibody region so that SNR could be calculated and a statistical analysis could be made. Table 7 summarizes the peak heights and standard deviation obtained with MATLAB. Statistical analysis shows that signal from each peak region is statistically greater than background ($p < 0.005$). It should be noted that the 9BG5 antibody region for level 3 testing of T3SA+ shows a statistically significant signal increase over the negative control region using this MATLAB analysis. However, this is merely a result of slight fluctuations in the background signal along the filament length, including a slight dip of the signal in the negative control region. A close inspection of the data set show that the apparent peak is merely an artifact which is suggested by the low calculated SNR of 1.1. No peak was found using the LabView detection program for this region.

Table 7: Average and standard deviation of peak heights determined by MATLAB. SNR was calculated by dividing average peak voltage by the average negative control voltage. All peaks were shown to be statistically significant with $p < 0.005$. *The peak corresponding to level three detection of T3SA+ was not found by LabView, but noise present in the background signal was great enough to create a false positive during MATLAB analysis.

Virus	Level	Peak Height (voltage)	SNR	Statistically Significant?
T3D	1	0.78 ± 0.071	11.5	Yes
	2	1.1 ± 0.12	9.8	Yes
	3	0.47 ± 0.057	3.3	Yes
T3SA+	1	1.17 ± 0.12	8.8	Yes
	2	0.35 ± 0.081	8.3	Yes
	3	0.052 ± 0.006	1.1	Yes*
T1L	1	0.344 ± 0.062	6.4	Yes
	2	0.39 ± 0.048	5.1	Yes
M13K07	1	6.44 ± 1.03	88	Yes

Discussion

FARA was first reported using immobilized anti-M13 antibody regions to detect the presence of M13K07 phage (43). This virus and antibody pair provided a well-characterized test system to show the feasibility of a filament-based virus detection platform; however, filaments needed to be removed from the system for fluorescence scanning. Further improvements were made to FARA that included an integrated fluorescence detector, so filaments could be immediately scanned for fluorescence, and results could be passed back to the filament control program (62). The integrated detector allowed for adaptive virus detection where regions of interest along the filament could be re-incubated in the appropriate reaction chambers to increase filament fluorescence when the initial signal was too low.

In this report, we utilize the unique feedback capability to guide additional testing based on the current results. Following the five-step incubation in the reaction chambers, the LabView VI immediately scans the region of interest for fluorescence. This data is then used to make a diagnosis based on the known locations of immobilized antibody regions. Figure 18 summarizes the theoretical decision tree resulting from the VI programming. Using online fluorescence detection and signal feedback, we were able to progressively diagnose the presence of reovirus with greater specificity at each level of testing (Table 6).

FARA relies on the ability of passively adsorbed antibodies on the surface of a monofilament to capture virus from solution. The use of a fluorescently labeled detection antibody that recognizes bound virus results in localized fluorescence from that region. The ability of bound antibody to retain its functionality is critical to the success of this

system. Each of our immobilized test antibodies retained their functionality and could detect a reovirus concentration of 2 x 10^{12} virions/ml as shown in Figure 19. Distinct peaks are present for each immobilized antibody region when incubated with its corresponding virus. The absence of peaks in the negative control regions and in non-specific antibody regions shows that cross reactivity is not a problem for this system.

It is clear from Figure 19 that detection of reovirus is possible using FARA, but our filament control program in LabView must automatically find each peak, calculate its location along the filament, and make a decision regarding additional tests based on the diagnosis. The LabView peak detector VI uses an algorithm that fits a quadratic polynomial to sequential sets of points, depending on the width parameter entered by the user. The data is then compared to the threshold parameter, also entered by the user, to determine peaks. Our LabView VI then makes a binary decision to stop or continue testing based on the location and number of peaks found. For each virus tested, LabView found the appropriate peaks, returned the appropriate diagnosis, and continued testing when necessary. Table 6 summarizes the results from these automated experiments using each of the four test viruses. For multilevel experiments (T3D, SA+, T1L), results in Table 6 represent single filaments with multiple test regions.

To ensure that LabView peak detection represented peak values that were statistically significant over background, data curves were analyzed externally using MATLAB. The mean and standard deviation from peak regions and negative control regions were compared to calculate SNR and statistical significance. In all cases where LabView found peaks, SNR was calculated to be greater than three, and fluorescence differences between peak and negative control regions were all statistically significant (p

< 0.005) as shown in Table 7. However, this table shows a statistically significant peak not found by LabView in the 9BG5 region of T3SA+ level 3 testing. Level 3 testing uses AF555-4F2 as the detecting antibody, so no peak should be present using this virus. Although SNR is only 1.1, the resulting p-value is less than 0.005. Close inspection of the data show that this is merely an artifact of fluctuating background noise, including a slight dip the background in the negative control region. MATLAB analysis of the data proves that LabView has not produced any false positives and all peaks represent statistically significant increases in signal over background.

Accurate positioning of the filament is another major issue of multilevel testing. For level one testing, the first test region can be positioned manually before the experiment begins. However, for subsequent testing, the VI needs to keep track of filament position so it knows when the second testing region is located in chamber 1. This was achieved with a very simple bar code system using the same fluorescent markers used to identify each region of interest. After a region is scanned, the program moves the filament forward until a known pattern of fluorescent markers is detected, indicating that the next region is located in chamber 1 for testing. Since our system only involved three levels, the program searched for one or two marks corresponding to levels two and three, respectively. However, it would be easy to incorporate more complex bar codes using additional spots or patterns of spots for more complicated systems.

Reovirus is typically used to study the mechanisms of viral infections and viral pathogenesis in mice. Although it is a human pathogen, it is rarely associated with adult human disease(28,30,31). Many reovirus field isolates have been very well characterized and a broad array of antibodies are available that recognize reovirus with varying

specificity, which is a requirement of our approach (66). For these reasons, reovirus was a suitable test system to show clinical relevance to this system, while alleviating some safety concerns in the laboratory. However, we observed an interesting phenomenon while testing the reovirus antibodies. Not every antibody was suitable for use as an immobilized primary antibody. Neither 8H6 or 4F2 antibody yielded positive results when used as the primary antibody, even if virus incubation time was dramatically increased (results not shown). It is possible that these antibodies undergo more extreme conformational changes than other antibodies when passively adsorbed to a solid substrate, rendering them inactive. However, a more likely cause is the location of the proteins they recognize on the reovirus surface (28,66). 8H6 and 4F2 recognize the μ1c and σ3 proteins from the outer capsid surface of the virion. Each virion contains approximately 600 copies of each protein on the surface of the viral core, but their are λ2 proteins arranged as pentamers extending outward from the surface of the core with oligomers of the σ1 protein extending even further. It is possible that these extensions from the virion core are sterically hindering the surface μ1c and σ3 proteins from getting close enough to the filament surface to bind to the 8H6 and 4F2 antibodies. The same reasoning could explain why 9BG5 and 5C6 were both excellent primary antibodies since they recognize the σ1 protein that extends furthest from the viral core. The inability of 8H6 and 5C6 antibodies to be effective primary antibodies complicated our virus detection scheme. Since 8H6 is non-serotype specific and should bind all reovirus, we had to find an alternative immobilized antibody for level 1 testing. 5C6 and 9BG5 antibodies are serotype specific for type 1 and type 3, respectively, so immobilizing a mixture of these was effective for general reovirus detection in level 1. Although 4F2 is

typically specific for all type 3 reovirus, T3SA+ is a reassortant mixture of type 1 and type 3 reovirus that contains the σ3 gene segment from type 1. As a result, 4F2 did not recognize T3SA+ and was specific only for T3D in our scheme. Since 4F2 could not be used as a primary antibody in level 3, we incorporated a fluorescently labeled 4F2 antibody as the detecting antibody and used a separate channel for detection. When these antibodies are in solution trying to bind to an already bound virus, steric hindrance is no longer an issue.

Conclusion

We have shown the feasibility of a programmable, completely automated system for diagnosing specific reovirus subtypes. Although the scheme we report is a relatively simple example of this, a much more complicated design could be easily envisioned. Each region used for testing could contain many more antibody regions that currently used, and there is effectively no limit to the overall length of the filament that could be used, so dozens of testing regions could be incorporated into one long filament. The most important requirement is the availability of a full panel of antibodies with a wide range of specificity. Many of the issues concerning primary antibodies and steric hindrance could be surpassed by alternative linking strategies to the filament. Using a flexible linker such as poly-l-lysine or other polymer would confer some freedom of movement for immobilized antibodies, negating the effects of steric hindrance for bulky viruses.

CHAPTER VI

CONCLUSIONS AND FUTURE WORK

Potential Applications

As mentioned previously, this technology could be very useful for probing a biological sample for numerous viruses in clinical setting. However, one could easily envision use of this technology in the area of biodefense. The ability of the filament to probe huge volumes could make it a good candidate for detecting airborne pathogens. The filament could be woven into a mesh-like configuration to increase surface area exposed to air. Following exposure, the mesh could be unraveled and sent through the system of reaction chambers for processing. Although airborne pathogens would probably be present in extremely low concentrations, huge volumes of air could be collected with a vacuum system and passed over the mesh of antibody probes serving as a course filter. In this way, very low concentrations of airborne pathogens could be detected. Probes representing many common biological threats could be immobilized on the mesh framework to create a "universal" biowarfare detection kit that is only limited by the availability of effective antibodies to each threats.

This technology could also be useful for environmental monitoring. Similar to the biowarfare detection kit, probes specific for common pollutants could be immobilized on the filament. The filament could then be dragged through a reservoir and processed to monitor levels of various pollutants. Again, the ability to probe large volumes will help detect molecules of interest that may be present only in low concentrations. Monitoring byproducts and or pollution in pipe flow would also be a very attractive application for

the system. Running the filament through the pipe and positioning the probe of interest in the middle of the flow could allow monitoring of numerous compounds. Probes could be processed and reprocessed at set time intervals until the signal of interest reaches a set level. Possible applications for this system are countless, but an ideal application would be able to take advantage of every unique property of this system, including the flexibility, sensitivity, and efficiency, and would be able to take advantage of the feedback system.

Future Work

Many areas of this technology remain to be fully explored. The sensitivity of this system is something that can always be improved further. Different primary antibody immobilization techniques could prevent much of the antibody functionality loss that results from passive adsorption to a solid substrate. Site-specific attachment of the antibody to the filament would greatly increase antibody functionality by leaving the binding sites free for antigen binding, and flexible linker arms could eliminate the effect of steric hindrance that was problematic for some antigen/antibody combinations.

Other detection strategies could also benefit our detection platform. The use of quantum dots, for example, could increase fluorescence due to their high quantum yield. In addition, the resistance to bleaching, the wide array of colors that are available, and the ability to excite them all using a single excitation source might make them an attraction detecting molecule over fluorescent dyes. Multiple detection channels could be incorporated simply by integrating an emission filter wheel in between the sample chamber and photomultiplier.

Alternative designs for the glass sample chambers could also greatly improve the functionality of the system. Incorporating some fluidics into the chambers would allow easy flushing of chambers in between experiments, so fluid loss from chambers would no longer be a problem. Detecting molecules could be introduced to the chambers before each experiment rather than in a mixture at the beginning of testing.

Incorporating DNA into this detection system represents a major avenue of research that has not yet begun. Although linking strategies and incubation steps may differ for DNA detection, most of the principles and core components of the system could remain the same. DNA detection would show an even greater level of flexibility of this assay and would open up even more applications for this platform.

There are many possible avenues to explore that could improve this technology or expand the potential applications of this technology, but it is not feasible to list them all here. However, the previous work on this system has provided a solid base from which to launch new areas of research and development.

APPENDIX A

MONOFILAMENT PROPERTIES AND SELECTION

Table 8: Physical and chemical characteristics of some potential filaments. Of these, the Sulky Invisible and Text-Dev PP were chosen initially for their combination of minimal autofluorescence, excellent flexibility, chemical compatibility, and size.

Filament	Composition	Diameter (μm)	Autofluorescence				Flexible	Organic compatibility
			Cy3	Cy5	Fluorescein	Rhodamine		
Spiderline super mono	Polyethylene?	270	N	N	N	N	Y	Y
Glass Fiber Optic	Glass	400	N	N	N	N	N	Y
Stren	PVDF	410	N	N	Y	N	Y	Y
Ande#6	Nylon mix	180	Y	N	N	N	Y	Y
Dupont 0.012	Nylon	300	Y	N	N	N	Y	Y
Silk thread	Silk	170	N	N	N	N	Y	Y
Wonder Invisible	Nylon	90	Y	N	N	N	Y	Y
Sulky Invisible	Polyester	120	N	N	N	N	Y	Y
Text-Dev PP	Polypropylene	180	N	N	N	N	Y	Y

Four key characteristics of the ideal monofilament were identified and were used to evaluate nine commercially available filaments. The four main criteria included diameter, autofluorescence using four different filter cubes, flexibility, and organic solvent compatibility. Common filaments are made of various materials such as polyethylene, polyester, nylon, glass, PVDF, and silk. Probe immobilization has not been extensively studied on any material other than polystyrene and glass, so the composition of potential filaments was not a factor other than the way in which it affected our four criteria. In addition, all of these materials (except silk thread) exhibited adequate strength

and abrasion resistance, so this was also not a factor in choosing the filament other than eliminating silk thread as an option. The results are summarized in Table 8.

Autofluorescence was determined by taping each filament to a glass slide and imaging them under an inverted fluorescence microscope using filter sets corresponding to Cy3, Cy5, fluorescein, and rhodamine. Any filament that showed significant fluorescence using any one of these filter sets was immediately discarded. The flexibility required is only enough to wrap around a 3/4" spool attached to the prototype motor shaft. All of the polymer filaments easily met this requirement, but the glass optical fiber became much too brittle after the protective plastic cladding was removed. Organic compatibility was estimated by soaking the filaments in various organic solvents that could potentially be used as liquid valves for our chambers. Liquid valves are organic liquids that may be used to seal the ends of the reaction chambers to prevent fluid loss and will be discussed later. All of the filaments appeared to have adequate solvent compatibility.

For the three remaining possible filaments under 200 μm (Wonder Invisible, Sulky Invisible, Text-Dev PP), autofluorescence was tested again using our GenePix 4000B microarray scanner to increase sensitivity of the test. This testing revealed that the Wonder Invisible nylon filament displayed 2-3 times the autofluorescence in the Cy3 channel than the Sulky Invisible filament, which had 2-3 times the autofluorescence of the polypropylene, making the polypropylene the best initial choice.

One filament characteristic that merits further discussion is that of filament diameter. The optimal filament diameter is partly influenced by the diameter of our reaction chambers. Since a major benefit of the system is greatly reduced diffusion distance for

target molecules, an ideal filament diameter should be very close to the chamber diameter to minimize this distance. Therefore, from this standpoint, available filament and chamber diameters will determine the sizes of each that are chosen. However, filament diameter also may have an effect on assay sensitivity independent of chamber size. This system immobilizes probe around the entire circumference of the filament and, theoretically, will bind virus and detecting antibody around the entire circumference, as well. However, since our excitation light source shines only on one side of the filament, it is not clear how much signal is detectable from the opposite side. The absorbtivity of the fiber is still unknown to us. Attempts thus far to measure this property on a UV/VIS spectrophotometer have been unsuccessful. If absorption is significant, then the filament diameter obviously plays an important role in determining how much excitation light will reach the opposite side of the filament. The current filament of choice is transparent, so we do not believe that absorption of visible excitation light is a major problem.

As stated above, the polypropylene filament fulfilled many of the identified requirements for this system, however a major question remained concerning the ability of polypropylene to passively bind protein. Therefore, both polypropylene and polyester filaments were used for testing. Although both polypropylene and polyester filaments were both found to adequately bind antibodies, the polypropylene filament often resulted in less defined, splotchy filament fluorescence during virus detection experiments.

APPENDIX B

CHAMBER DESIGN AND FLUID LOSS

Chamber design was critical for optimizing the signal and maintaining consistent results within runs and between runs. We identified three important parameters involved with this part of our experimental design. First, the size of the chamber should minimize reaction volumes and diffusion distance for target molecules, so that the time required for maximum probe/target interaction is short. Next, the chamber should be designed to minimize fluid loss to the environment. Third, it should be made out of a material that will not react with or hinder binding between probes and targets and should also allow monitoring of fluid levels within.

For the preliminary studies, chambers were made from 700 μm ID, 25 μl capillary tubes to avoid difficulties of working with very small tubes. Even with this relatively large capillary tubing, diffusion distance for target molecules is still very small compared to most array techniques. The maximum radial diffusion from the filament to the wall of the capillary is only 290 μm, compared to over 1 cm for most array techniques; however, the time scale for diffusion of this distance is still much too large. Assuming diffusion constants of $1x10^{-7}$ and $1x10^{-6}$ (20-22), a simple calculation predicts approximately 2 hrs and 0.2 hrs, respectively, to achieve that distance. Significantly smaller capillary tubing is available, but durability for these small capillaries is a major problem. To improve the durability of reaction chambers, we used 1/4" stock glass tubing that is availability in several different inner diameters and cut it into 75mm lengths. This tubing improved the

strength of these chambers, and made filling, emptying, and washing of the chambers much easier. Much smaller inner diameter tubing is available that would reduce the diffusion distance even further and reduce the required filling volume to only a few microliters.

Initial experiments were performed with open-ended capillaries; however, fluid loss to the environment was a potential problem with this design. Evaporation from the capillaries was limited to approximately 5% from each end during a two hour mock experiment when the filament was not pulled through the interior, but passage of the filament through the lumen caused fluid loss to approach 15% from each end, which is a significant problem. The use of organic liquid valves initially appeared to be a relatively simple solution that we explored. A very small volume of an organic liquid placed at the ends of the reaction chambers could prevent fluid loss when the liquid is one that has very low vapor pressure and high surface tension. The former will inhibit evaporation while the latter will keep the valve in place and prevent reaction fluids from contaminating adjacent chambers as the filament is pulled through. Figure 21 displays surface tension and vapor pressure values for numerous common organic solvents. Propyl benzoate was initially chosen due to its high surface tension and low vapor pressure, but initial attempts at integrating this compound as a liquid valve were not successful. It has been suggested that antibody tertiary structure is disrupted at the organic/aqueous interface (67), which may prevent binding of probes to targets. We have identified some other candidates that may be effective as liquid valves such as mineral oil and glycerol that are known to be biocompatible with proteins and should not disrupt protein folding. These experiments have not yet been performed.

A second solution involved placing short lengths of heat-shrink tubing on the ends of each capillary. Although the final size of the heat-shrink tubing was only slightly smaller the capillaries, it reduced fluid loss significantly. In fact, fluid loss using this solution was diminished to the point where it is approximately equaled the static system with no filament movement. As we incorporated the larger OD tubing, it was no longer feasible to use heat-shrink tubing to minimize fluid loss. We initially designed some chambers with a narrow neck at each end that should have the equivalent effect of the heat shrink tubing. However, the narrow neck negatively affected virus detection, probably though increased shear stress as the filament passed through the chambers. Our final design eliminated the narrow neck in favor of an outward flare at each end. The flared end appeared to help minimize fluid loss through capillary effects, indicating that much of the fluid loss was caused by the filament "pulling" solution from the chambers.

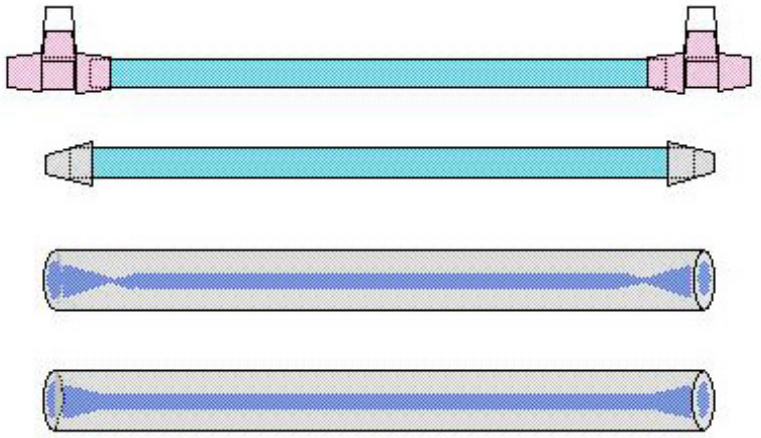

Figure 20: Four chamber designs used for virus detection. Liquid valves are depicted in the top design followed by the heat shrink tubing design, narrow-necked chambers, and simple flared chambers at the bottom.

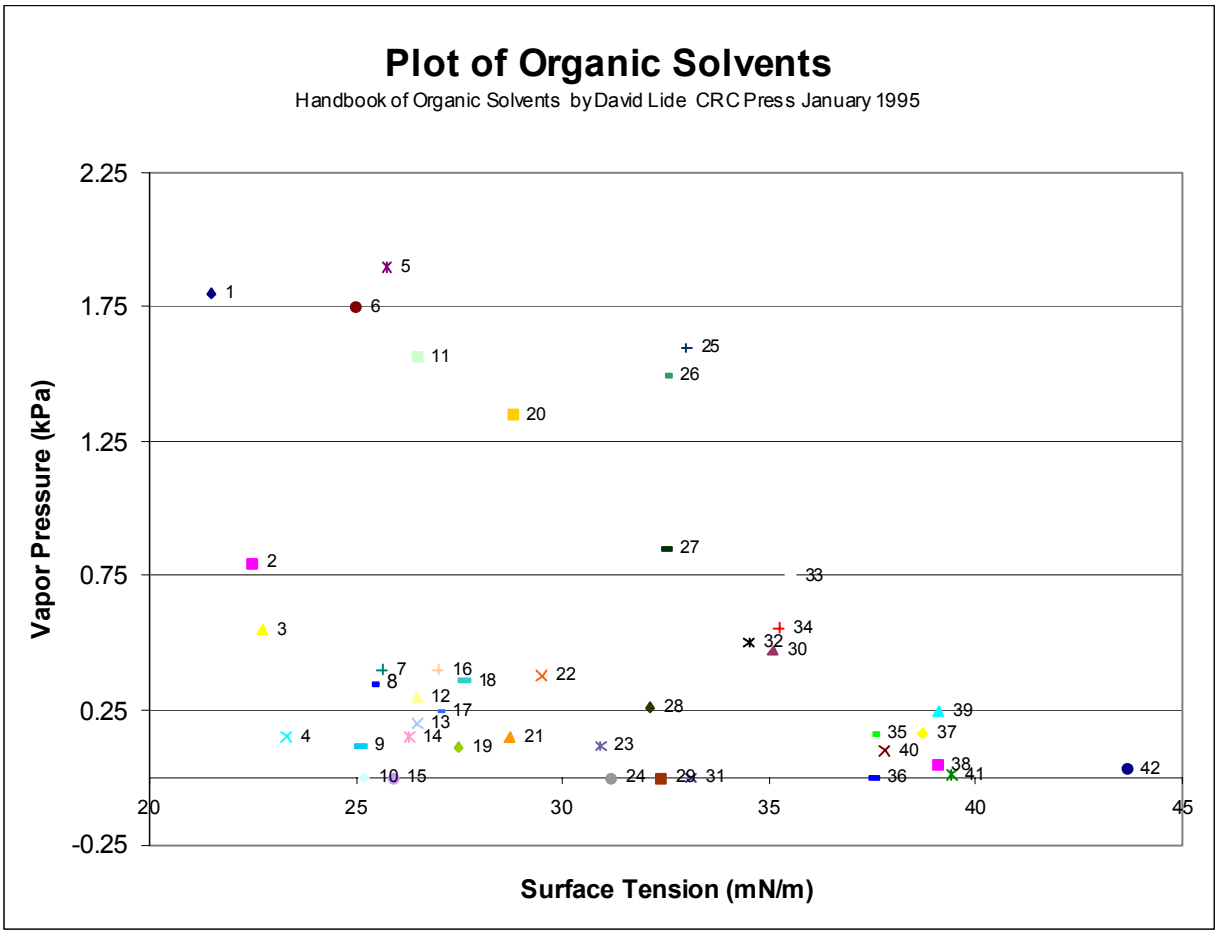

Figure 21: Surface tension and vapor pressure values for many common organic solvents. Propyl benzoate (#39) was initially chosen as a liquid valve due to its high relative surface tension, low vapor pressure, and availability.

APPENDIX C

EFFECT OF SHEAR STRESS ON VIRUS DETECTION

Table 9: Shear stress calculations using a four different chamber sizes and three different filament speeds.

		Shear Stress (Pa)		
Chamber Diameter (μm)	Wall to filament Dist (m)	2 cm/sec	1 cm/sec	0.5 cm/sec
200	4.00E-05	0.500	0.250	0.125
300	9.00E-05	0.222	0.111	0.056
750	3.15E-04	0.063	0.032	0.016
1000	4.40E-04	0.046	0.023	0.011

Shear stress = (dynamic viscosity x filament velocity) / distance to wall
Dynamic viscosity = 1 x 10^{-3} Ns/m^2 (same as water)
Filament diameter = 120 μm

Since shear stress created by filament movement may reduce virus binding, an estimation of shear stress was made based on filament movement parameters within the capillary chambers. Shear stress is equal to the product of dynamic viscosity and filament velocity divided by distance between filament and capillary wall (68). Assuming a dynamic viscosity equal to water at 20°C ($1x10^{-3}$ $N{\cdot}s/m^2$), shear stress resulting from moving the filament 1 cm/sec in a 750 μm chamber is approximately 0.3 $dynes/cm^2$ (0.03 Pa). This low level of shear stress should not significantly affect antigen/antibody interactions. This calculation is based on perfect concentricity of the filament within the chamber, so the actual shear may vary from that value, depending on the position of the filament. However, even if misalignment of the filament reduces the

distance between the filament and wall by a factor of 100, the shear stress is still relatively low. Many reports in the literature show reduced antigen binding as a result of shear stress, but most of these studies use shear stress that are several orders of magnitude greater than what is present in this FARA system (69). It does not appear that any further reductions in chamber size or misalignment of the filament will create a high enough shear stress to have a negative effect on virus detection using our current filament movement parameters.

We tested glass chambers with a narrow neck at each end of approximately 200 μm that were designed to minimize fluid loss. Several of these experiments used a global filament movement speed of 2 cm/s. Qualitative analysis of these experiments showed that the combination of a very small neck and higher filament speed had a negative impact on virus detection. All subsequent experiments used flared chambers rather than necked and filament speed was limited to 1 cm/s.

APPENDIX D

LIGHT ACTIVATED ANTIBODY COUPLING

The theory behind the following experiments is explained by Holden and Cremer in "Light Activated Patterning of Dye-Labeled Molecules on Surfaces" (70). The first experiment shows that FITC labeled anti-M13 can be attached to the polyester filament using the UV gel box. In that experiment, the entire filament was incubated with FITC labeled anti-M13, but only the three green regions were exposed to UV light. The antibody was successfully immobilized only in the three exposed areas. There is a lot of remaining green fluorescence showing that the FITC was not completely bleached (top panel of Figure 22). The subsequent virus detection experiment using this filament did not work as shown in the lower panel of Figure 22 where red fluorescence is not seen. See GS Lab Book #6, 8-3-05, p. 51 for details of this experiment.

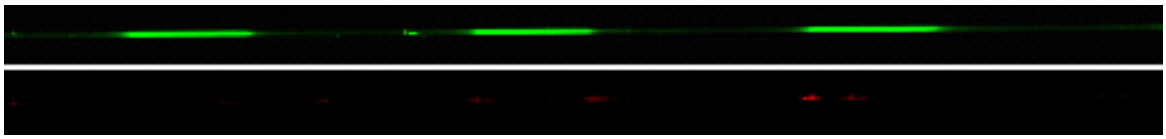

Figure 22: Filament fluorescence after using gel box to bleach FITC labeled antibody onto the filament. Green fluorescence shows that FITC anti-M13 is attached to the filament but did not get completely bleached. This filament was used in a virus detection experiment, but did not successfully detect virus as shown by the lack of red fluorescence in the bottom picture.

The second experiment described here contained three sets of three antibody spots followed by a negative control (Figure 22). The first set contained three FITC anti-M13 regions that were bleached onto passively adsorbed fibronectin. The second set was

FITC bleached directly onto the filament. The third set was the typical passive adsorbtion used in most experiments, and the final spot is a negative control anti-E spot. Average spot fluorescence from each set was similar, but the passively adsorbed set appeared less defined than the bleached regions. This observation was seen in several experiments comparing passive adsorption to bleaching. See Kelvin Lab Book #1, p. 85 for details of this experiment along with fluorescence values. For additional bleaching experiments, see Kelvin Lab Book #1, p. 83-86, 92-93. More testing is necessary to determine the value in bleaching antibody regions on the filament, but it appears to create more defined antibody regions.

Figure 23: Virus Detection results using bleached filament. Passively adsorbed anti-M13 regions appeared less defined than bleached regions. The presence of fibronectin in bleached regions did not appear to have an effect. Average fluorescence intensity from the three different treatments was similar.

APPENDIX E

GOLD FILAMENTS

The following experiments show the potential gold as a substrate for virus detection experiments. The true value of using a gold substrate is the easy covalent coupling of antibodies to gold using cysteine residues on the antibody. However, our experiments started only with passive adsorption to gold. The first experiment utilized a gold wire with five passively immobilized anti-M13 regions. The wire was then incubated offline in test tubes for each step and scanned on the microarray scanner. Figure 24 shows successful virus detection in all five antibody regions. See GS Lab book #5, 7-12-05, p. 41 for details on this experiment

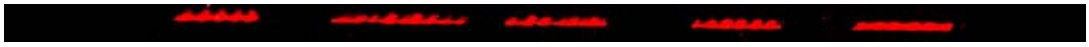

Figure 24: Gold wire showing virus detection using five regions of passively immobilized anti-M13 regions.

A major advantage of gold substrates is its electrical conductivity. This conductivity can be taken advantage of by applying a potential to the wire to attract oppositely charged antigens in solution to speed up antigen movement towards the surface of the wire. Using gel running buffer, we applied a either a positive or negative potential to the filament and compared virus detection results. All steps other than the virus incubation step were done offline in test tubes. The positive voltage should attract virus particles in a 1x gel running buffer, while a negative voltage should repel them. Figure 25 shows

that a positive voltage results in an increase in fluorescence of approximately 30x over negative voltage. See GS Lab Book #5, 7-21-05, p. 57 for details of this experiment.

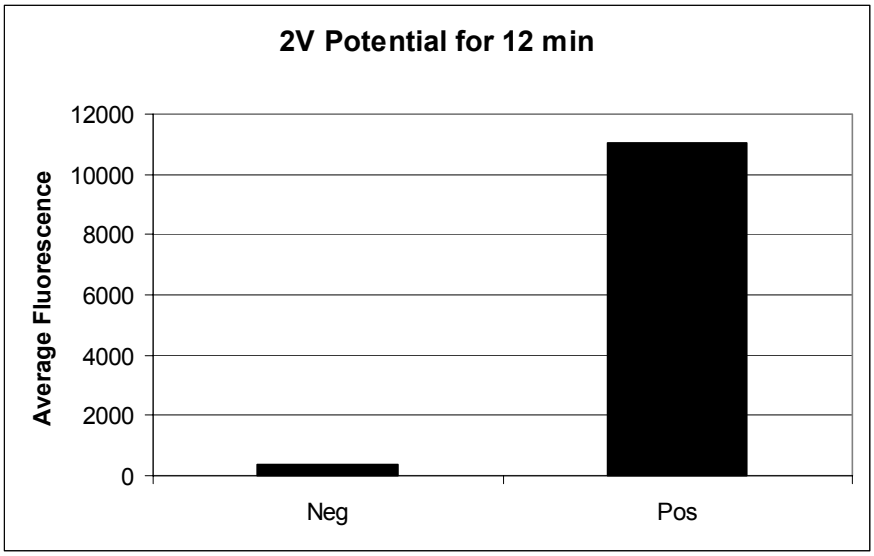

Figure 25: Virus detection using a gold wire with applied positive and negative voltages. Positive voltage on the wire increase fluorescence by a factor of approximately 30.

APPENDIX F

MATLAB CODE FOR AIM III

This MATLAB script was used in Aim III to find the average and standard deviation of the raw fluorescence data obtained through LabView. This code was written by Rob Brychta.

```
%greg_peak_detect2

close all, clear all, clc
%Choose a File
[filename, pathname, filterindex] = uigetfile( ...
       {'*.xls','Excel File (*.xls)';
       '*.txt','Text Files (*.txt)';...
        '*.*',  'All Files (*.*)'}, ...
       'Pick a file', 'Untitled.xls');
if (filterindex > 0)
   if (filterindex==1)
       cd(pathname);
       [numeric,txt,raw]=xlsread(filename);
       %cols = txt(2,:);  %This is where the column headings are (row number 2 for now)
       cols = txt(1,:);
       for i = 1:length(cols)
          id1(i) = strncmp('y',lower(cols(24)),1);
       end
       id1 = find(id1);
       numcols = length(id1);
       y = numeric(:,id1);

   elseif (filterindex == 2)
       cd(pathname)
       [header,tags,data] = read_txt_greg(filename,pathname);
       for i = 1:size(tags,1)
          id1(i) = strncmp('y',lower(tags(i,:)),1);
       end
       id1 = find(id1);
       numcols = length(id1);
       y = data(:,id1);
```

```
        y = cell2mat(y);
        y = str2num(y);
    end

    for i = 1:numcols
        ynew = y(:,i);
        nanid = isnan(ynew);
        nanid = find(nanid);
        ynew(nanid) = [];
        figure,
        plot(ynew)
        axis tight

        button = 1;
        ii = 1;
        while(button ~=3);
            waitfor(gcf,'CurrentCharacter',double('d')); %to zoom
            %select center of cell
            [xcoordt, ycoordt,button] = ginput(1);
            if (button == 3),
                break,
            else
                xcoord(ii) = round(xcoordt);
                ycoord(ii) = ynew(xcoord(ii));
                hold on, plot(xcoord(ii),ynew(xcoord(ii)),'r+')
                ii = ii+1;
            end
        end
        win = [-7:7];
        xmat = repmat(xcoord(:),1,length(win))+repmat(win,length(xcoord),1);
        xmat = xmat';
        pkmeans = mean(ynew(xmat));
        ycoord = ynew(xcoord);
        savename = [filename(1:find(filename=='.')-1) '_col_' num2str(i) '_pkmeans.mat'];
        save(savename,'xcoord','ycoord','pkmeans');
        clear xmat pkmeans ycoord xcoord ynew
        close(gcf);
    end

else
    msgbox('No File Selected')
end
```

APPENDIX G

LAB NOTEBOOK REFERENCES

Figure	Date of Experiments	Lab Notebook Reference
5 (top) 5 (bottom)	11-24, 11-25, 12-3-05 10-28-04	GS #4, p.72, 74, 78 GS #4, p.52
6	4-8-05	GS #4, p.154
7 (ELISA) 7 (FARA)	6-22-04 12-4 to 12-7-05	GS #5, p.36 GS #5, p.114
8	6-2 to 6-3-05	GS #5, p.8-11
11 (low power) 11 (high power dry) 11 (high power wet)	8-17-05 Dry: 5-17-05 Wet: 7-21-05	GS #6, p59-60 Kelvin #1, p.6 Kelvin #1, p.109
12	8-16-05	GS #6, p.56
13	8-24 to 8-25-05	OneNote, August 2005
14 (top) 14 (bottom)	8-18-05 8-23-05	GS #6, p.61 OneNote, August 2005
15	8-23 to 8-24-05	OneNote, August 2005
19 T3D 19 T3SA+ 19 T1L 19 M13K07	10-26-05 10-27-05 10-25-05 10-24-05	OneNote, October 2005

Table	Date of Experiments	Lab Notebook Reference
6	10-24 to 10-27-05	OneNote, October 2005
7	10-24 to 10-27-05	OneNote, October 2005

All data and results are organized by date in the “Filament Stuff” folder on Greg’s computer. GenePix images are organized by date in the “Stone” folder on the GenePix computer.

REFERENCES

1. **Reid, B.B.** 2002. NIH outlines goals to counter bioterror. Nature Biotechnology *20*:414-414.

2. **Dove, A.** 2002. Bioterrorism becomes one of the hottest US research fields. Nature Medicine *8*:197-197.

3. **Gonzales, R., D.C. Malone, J.H. Maselli and M.A. Sande.** 2001. Excessive antibiotic use for acute respiratory infections in the United States. Clin Infect Dis *33*:757-762.

4. 2002. Bioterrorism: Threat and Preparedness. *In*National Academy of Engineering.

5. **Jeffrey, K. and D. Pillay.** 2004. Diagnostic Approaches. *In* A. Zuckerman (Ed.), Principles and Practice of Clinical Virology. John Wiley & Sons, Hoboken, NJ.

6. **Niesters, H.G.** 2004. Molecular and diagnostic clinical virology in real time. Clin Microbiol Infect *10*:5-11.

7. **MacBeath, G.** 2002. Protein microarrays and proteomics. Nature Genetics *32*:526-532.

8. **Palmer, S., A.P. Wiegand, F. Maldarelli, H. Bazmi, J.M. Mican, M. Polis, R.L. Dewar, A. Planta, et al.** 2003. New real-time reverse transcriptase-initiated PCR assay with single-copy sensitivity for human immunodeficiency virus type 1 RNA in plasma. Journal of Clinical Microbiology *41*:4531-4536.

9. **Read, S.J., D. Burnett and C.G. Fink.** 2000. Molecular techniques for clinical diagnostic virology. J Clin Pathol *53*:502-506.

10. **Cheung, V.G., M. Morley, F. Aguilar, A. Massimi, R. Kucherlapati and G. Childs.** 1999. Making and reading microarrays. Nature Genetics *21*:15-19.

11. **Duggan, D.J., M. Bittner, Y.D. Chen, P. Meltzer and J.M. Trent.** 1999. Expression profiling using cDNA microarrays. Nature Genetics *21*:10-14.

12. **Schena, M., D. Shalon, R.W. Davis and P.O. Brown.** 1995. Quantitative Monitoring of Gene-Expression Patterns with a Complementary-DNA Microarray. Science *270*:467-470.

13. **Southern, E.M.** 1975. Detection of Specific Sequences among DNA Fragments Separated by Gel-Electrophoresis. Journal of Molecular Biology *98*:503-&.

14. **Brown, P.O. and D. Botstein.** 1999. Exploring the new world of the genome with DNA microarrays. Nature Genetics *21*:33-37.

15. **Southern, E., K. Mir and M. Shchepinov.** 1999. Molecular interactions on microarrays. Nature Genetics *21*:5-9.

16. **Lander, E.S.** 1999. Array of hope. Nature Genetics *21*:3-4.

17. **Lipshutz, R.J., S.P.A. Fodor, T.R. Gingeras and D.J. Lockhart.** 1999. High density synthetic oligonucleotide arrays. Nature Genetics *21*:20-24.

18. **Fodor, S.P.A., J.L. Read, M.C. Pirrung, L. Stryer, A.T. Lu and D. Solas.** 1991. Light-Directed, Spatially Addressable Parallel Chemical Synthesis. Science *251*:767-773.

19. **Schena, M., R.A. Heller, T.P. Theriault, K. Konrad, E. Lachenmeier and R.W. Davis.** 1998. Microarrays: biotechnology's discovery platform for functional genomics [see comments]. Trends Biotechnol *16*:301-306.

20. **Arrio-Dupont, M., G. Foucault, M. Vacher, P.F. Devaux and S. Cribier.** 2000. Translational diffusion of globular proteins in the cytoplasm of cultured muscle cells. Biophysical Journal *78*:901-907.

21. **Eimer, W. and R. Pecora.** 1991. Rotational and Translational Diffusion of Short Rodlike Molecules in Solution - Oligonucleotides. Journal of Chemical Physics *94*:2324-2329.

22. **Lapham, J., J.P. Rife, P.B. Moore and D.M. Crothers.** 1997. Measurement of diffusion constants for nucleic acids by NMR. Journal of Biomolecular Nmr *10*:255-262.

23. **Holloway, A.J., R.K. van Laar, R.W. Tothill and D.D.L. Bowtell.** 2002. Options available - from start to finish - for obtaining data from DNA microarrays. Nature Genetics *32*:481-489.

24. 2003. BD Clontech™ Antibody (Ab) Microarray 500. *In*.

25. **Schramm, W. and S.H. Paek.** 1992. Antibody Antigen Complex-Formation with Immobilized Immunoglobulins. Analytical Biochemistry *205*:47-56.

26. **Schramm, W., S.H. Paek and G. Voss.** 1993. Strategies for the Immobization of Antibodies. Immunomethods *3*:93-103.

27. **Butler, J.E., L. Ni, R. Nessler, K.S. Joshi, M. Suter, B. Rosenberg, J. Chang, W.R. Brown, et al.** 1992. The Physical and Functional-Behavior of Capture Antibodies Adsorbed on Polystyrene. Journal of Immunological Methods *150*:77-90.

28. **Dermody, T.S.** 1997. Reovirus, pp. 669-699. *In* N. Nathanson (Ed.), Viral Pathogenesis. Lippincott-Raven, Philadelphia.

29. **Nibert, M.L., D.B. Furlong and B.N. Fields.** 1991. Mechanisms of Viral Pathogenesis - Distinct Forms of Reoviruses and Their Roles During Replication in Cells and Host. Journal of Clinical Investigation *88*:727-734.

30. **Nibert, M.L., L.A. Schiff and B.N. Fields.** 1996. Reoviruses and their replication, pp. 1557-1596. *In* B.N. Fields, D.M. Knipe and P.M. Howley (Eds.), Fields virology. Lippincott-Raven, Philadelphia.

31. **Tyler, K.L. and B.N. Fields.** 1996. Reoviruses, pp. 1597-1623. *In* B.N. Fields, D.M. Knipe and P.M. Howley (Eds.), Fields Virology. Lippincott-Raven, Philadelphia.

32. **Owen, W.E. and W.L. Roberts.** 2003. Comparison of five automated serum and whole blood folate assays. Am J Clin Pathol *120*:121-126.

33. **Stern, P., B. Friedecky, V. Bartos, D. Bezdickova, J. Vavrova, J. Uhrova, L. Rozprimova, T. Zima, et al.** 2001. Comparison of different immunoassays for CA 19-9. Clin Chem Lab Med *39*:1278-1282.

34. **Iqbal, S.S., M.W. Mayo, J.G. Bruno, B.V. Bronk, C.A. Batt and J.P. Chambers.** 2000. A review of molecular recognition technologies for detection of biological threat agents. Biosensors & Bioelectronics *15*:549-578.

35. **Reischl, U.** 1996. Application of molecular biology-based methods to the diagnosis of infectious diseases. Front Biosci *1*:e72-77.

36. **Mubammad-Tahir, Z. and E.C. Alocilja.** 2003. A conductometric biosensor for biosecurity. Biosensors & Bioelectronics *18*:813-819.

37. **Ronkainen-Matsuno, N.J., J.H. Thomas, H.B. Halsall and W.R. Heinemann.** 2002. Electrochemical immunoassay moving into the fast lane. Trac-Trends in Analytical Chemistry *21*:213-225.

38. **Baselt, D.R., G.U. Lee and R.J. Colton.** 1996. Biosensor based on force microscope technology. Journal of Vacuum Science & Technology B *14*:789-793.

39. **Balasubramanian, A., B. Bhuva, R. Mernaugh and F. Haselton.** Si-based Sensor for Virus Detection. IEEE Sensor Journal (in press 2004).

40. **Plowman, T.E., J.D. Durstchi, H.K. Wang, D.A. Christensen, J.N. Herron and W.M. Reichert.** 1999. Multiple-analyte fluoroimmunoassay using an integrated optical waveguide sensor. Analytical Chemistry *71*:4344-4352.

41. **Ligler, F.S., C.R. Taitt, L.C. Shriver-Lake, K.E. Sapsford, Y. Shubin and J.P. Golden.** 2003. Array biosensor for detection of toxins. Analytical and Bioanalytical Chemistry *377*:469-477.

42. **Rowe, C.A., L.M. Tender, M.J. Feldstein, J.P. Golden, S.B. Scruggs, B.D. MacCraith, J.J. Cras and F.S. Ligler.** 1999. Array biosensor for simultaneous identification of bacterial, viral, and protein analytes. Analytical Chemistry *71*:3846-3852.

43. **Stone, G.P., R. Mernaugh and F.R. Haselton.** 2005. Virus detection using filament-coupled antibodies. Biotechnol Bioeng *91*:699-706.

44. **Peruski, L.F., Jr. and A.H. Peruski.** 2003. Rapid diagnostic assays in the genomic biology era: detection and identification of infectious disease and biological weapon agents. Biotechniques *35*:840-846.

45. **Andreotti, P.E., G.V. Ludwig, A.H. Peruski, J.J. Tuite, S.S. Morse and L.F. Peruski, Jr.** 2003. Immunoassay of infectious agents. Biotechniques *35*:850-859.

46. **Marazuela, M.D. and M.C. Moreno-Bondi.** 2002. Fiber-optic biosensors - an overview. Analytical and Bioanalytical Chemistry *372*:664-682.

47. **D'Orazio, P.** 2003. Biosensors in clinical chemistry. Clin Chim Acta *334*:41-69.

48. **Baselt, D.R., G.U. Lee, K.M. Hansen, L.A. Chrisey and R.J. Colton.** 1997. A high-sensitivity micromachined biosensor. Proceedings of the Ieee *85*:672-680.

49. **Balasubramanian, A., B. Bhuva, R. Mernaugh and F.R. Haselton.** 2005. Si-based sensor for virus detection. Ieee Sensors Journal *5*:340-344.

50. **Bramley, T.J., D. Lerner and M. Sames.** 2002. Productivity losses related to the common cold. J Occup Environ Med *44*:822-829.

51. **Heikkinen, T. and A. Jarvinen.** 2003. The common cold. Lancet *361*:51-59.

52. **Turner, R.B., M.T. Wecker, G. Pohl, T.J. Witek, E. McNally, R. St George, B. Winther and F.G. Hayden.** 1999. Efficacy of tremacamra, a soluble intercellular adhesion molecule 1, for experimental rhinovirus infection: a randomized clinical trial. Jama *281*:1797-1804.

53. **McIntosh, K.** 1999. Closer to a cure for the common cold? Jama *281*:1844-1845.

54. **Juven, T., J. Mertsola, M. Waris, M. Leinonen, O. Meurman, M. Roivainen, J. Eskola, P. Saikku, et al.** 2000. Etiology of community-acquired pneumonia in 254 hospitalized children. Pediatr Infect Dis J *19*:293-298.

55. **Makela, M.J., T. Puhakka, O. Ruuskanen, M. Leinonen, P. Saikku, M. Kimpimaki, S. Blomqvist, T. Hyypia, et al.** 1998. Viruses and bacteria in the etiology of the common cold. J Clin Microbiol *36*:539-542.

56. **Raty, R., T. Ziegler and M. Kleemola.** 2004. The value of virus serology in epidemiological studies of acute otitis media in children. J Clin Virol *29*:315-319.

57. **Vesa, S., M. Kleemola, S. Blomqvist, A. Takala, T. Kilpi and T. Hovi.** 2001. Epidemiology of documented viral respiratory infections and acute otitis media in a cohort of children followed from two to twenty-four months of age. Pediatr Infect Dis J *20*:574-581.

58. **Papadopoulos, N.G. and S.L. Johnston.** 2004. Rhinoviruses. *In* A. Zuckerman (Ed.), Principles and Practice of Clinical Virology. John Wiley & Sons, Hoboken, NJ.

59. **Schweiger, B., I. Zadow, R. Heckler, H. Timm and G. Pauli.** 2000. Application of a fluorogenic PCR assay for typing and subtyping of influenza viruses in respiratory samples. J Clin Microbiol *38*:1552-1558.

60. **Nyquist, A.C., R. Gonzales, J.F. Steiner and M.A. Sande.** 1998. Antibiotic prescribing for children with colds, upper respiratory tract infections, and bronchitis. Jama *279*:875-877.

61. **Mainous, A.G., 3rd, W.J. Hueston and J.R. Clark.** 1996. Antibiotics and upper respiratory infection: do some folks think there is a cure for the common cold. J Fam Pract *42*:357-361.

62. **Stone, G.P., K.S. Lin and F.R. Haselton.** 2006. Adaptive virus detection using filament-coupled antibodies. Journal of Biomedical Optics *Submitted for Review*.

63. **Barton, E.S., J.L. Connolly, J.C. Forrest, J.D. Chappell and T.S. Dermody.** 2001. Utilization of sialic acid as a coreceptor enhances reovirus attachment by multistep adhesion strengthening. J Biol Chem *276*:2200-2211.

64. **Chappell, J.D., J.L. Duong, B.W. Wright and T.S. Dermody.** 2000. Identification of carbohydrate-binding domains in the attachment proteins of type 1 and type 3 reoviruses. J Virol *74*:8472-8479.

65. **Furlong, D.B., M.L. Nibert and B.N. Fields.** 1988. Sigma 1 protein of mammalian reoviruses extends from the surfaces of viral particles. J Virol *62*:246-256.

66. **Virgin, H.W.t., M.A. Mann, B.N. Fields and K.L. Tyler.** 1991. Monoclonal antibodies to reovirus reveal structure/function relationships between capsid proteins and genetics of susceptibility to antibody action. J Virol *65*:6772-6781.

67. **Birdi, K.S.** 1989. Lipid and Biopolymers at Liquid Interfaces. Plenum Press, New York.

68. **Fox, R. and A. McDonald.** 1998. Introduction of Fluid Mechanics. John Wiley & Sons, Inc., New York.

69. **Harrison, J.S., A. Gill and M. Hoare.** 1998. Stability of a single-chain Fv antibody fragment when exposed to a high shear environment combined with air-liquid interfaces. Biotechnol Bioeng *59*:517-519.

70. **Holden, M.A. and P.S. Cremer.** 2003. Light activated patterning of dye-labeled molecules on surfaces. J Am Chem Soc *125*:8074-8075.